Micro-strip based detection systems: advances and new technological developments

Yoshinobu Unno
KEK

Your Lecturer

Yoshinobu UNNO

Your Lecturer

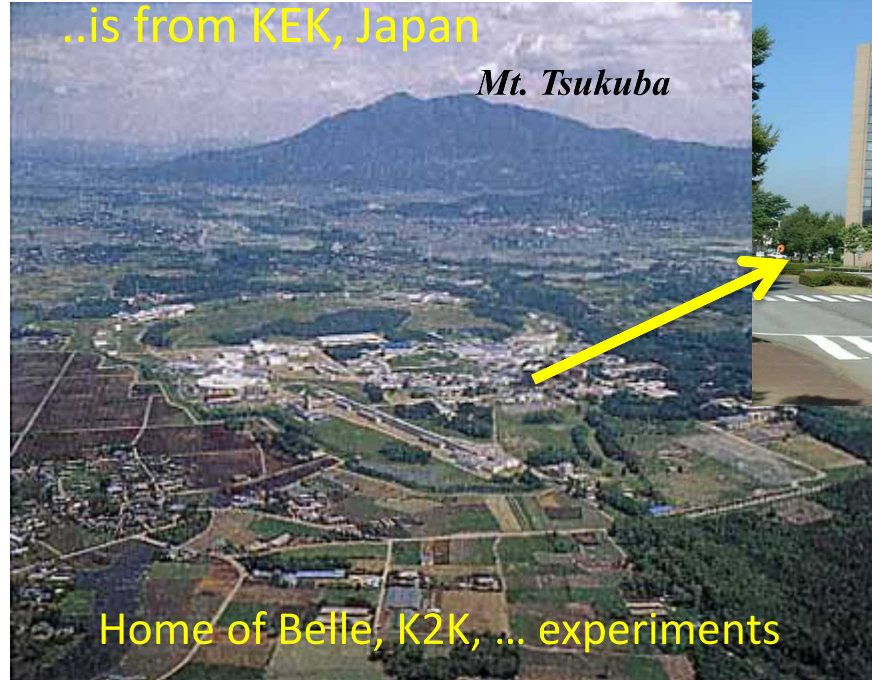

Yoshinobu UNNO
Professor of KEK

Your Lecturer

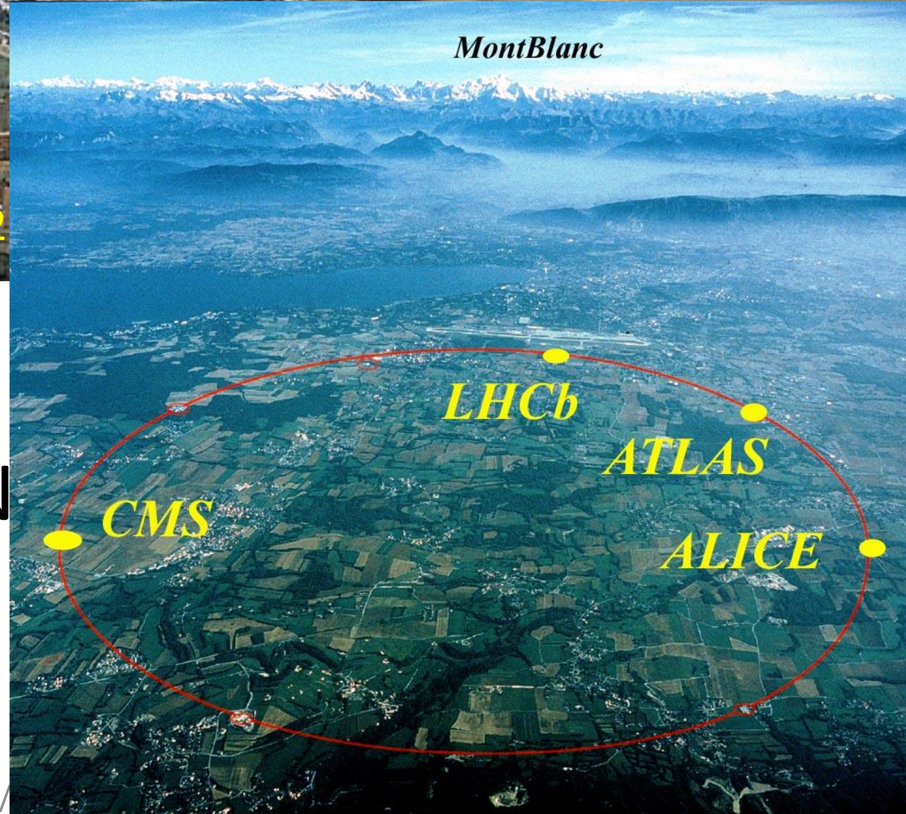

Yoshinobu UNNO
Professor of KEK
ATLAS experiment at CERN

Your Lecturer

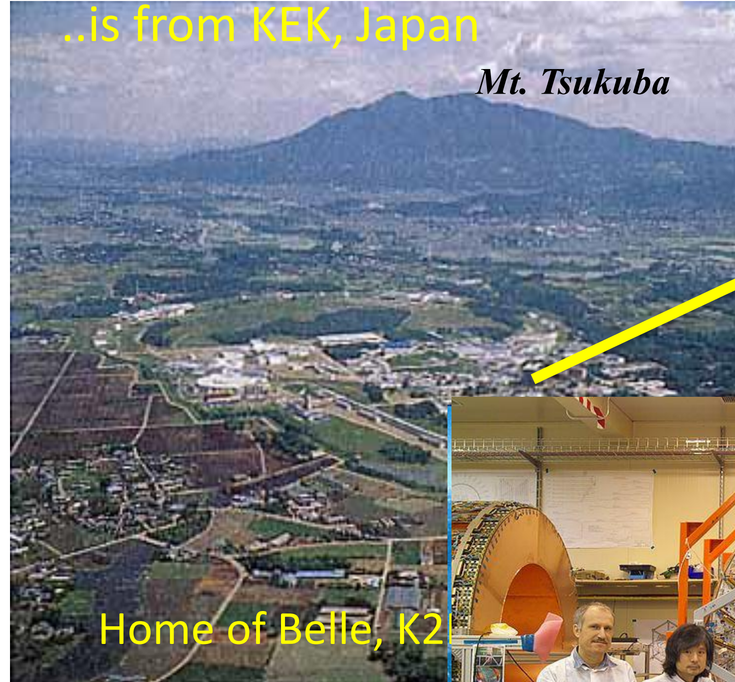

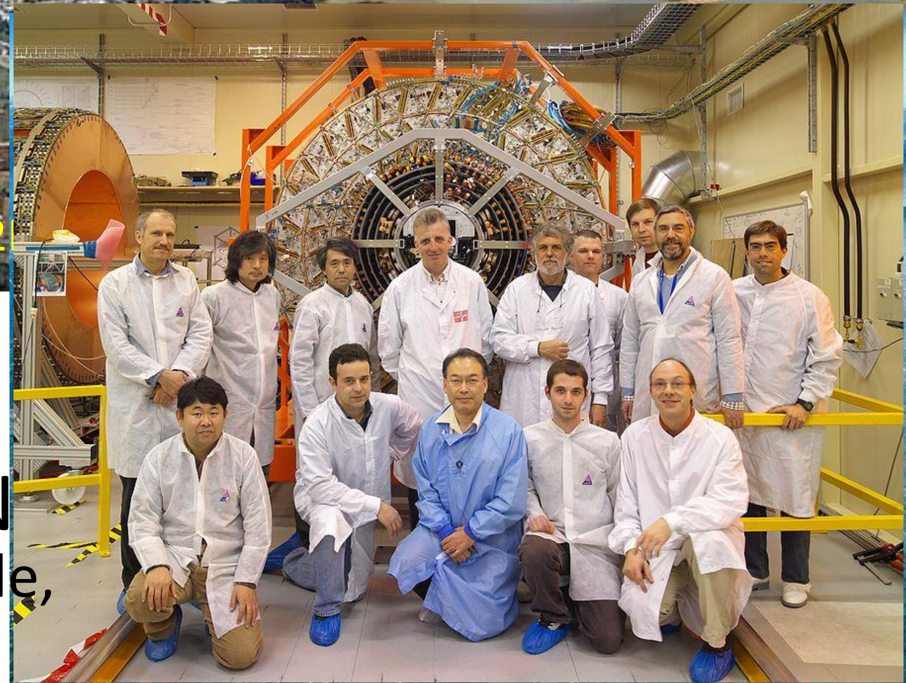

Yoshinobu UNNO
Professor of KEK
ATLAS experiment at CERN
Design, construction, … and upgrade, of the silicon tracker
- together with many colleagues
- for the great discovery

Japan - Wonderland

One of the advantage is the industry, specially electronics

Japan - Wonderland

Big electronics giants like HITACHI, …

Japan - Wonderland

Big electronics giants like HITACHI, SONY, …

Japan - Wonderland

HAMAMATSU

Photon is our business

SOLID STATE DIVISIONS

ELECTRON TUBE DIVISIONS

LASER GROUP

SYSTEM DIVISIONS

SONY

make.believe

TELEVISION AND A BLU-RAY PLAYER

HITACHI

Inspire the Next

私たち日立グループは柏レイソルを応援しています。

「日立の樹」www.hitachinoki.net

But, we have benefitted from a smaller company …

Japan - Wonderland

Nobel prize for opening the Neutrino astronomy

who has a long history of collaboration with our fields …

Japan - Wonderland

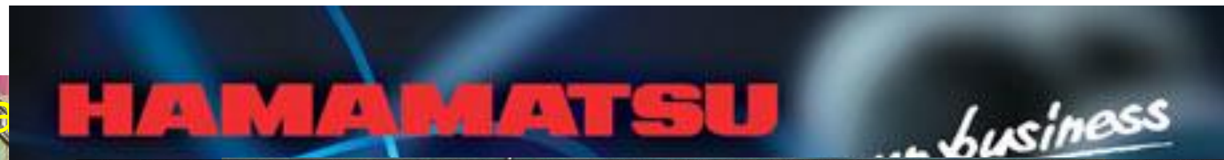

ATLAS Supplier Award

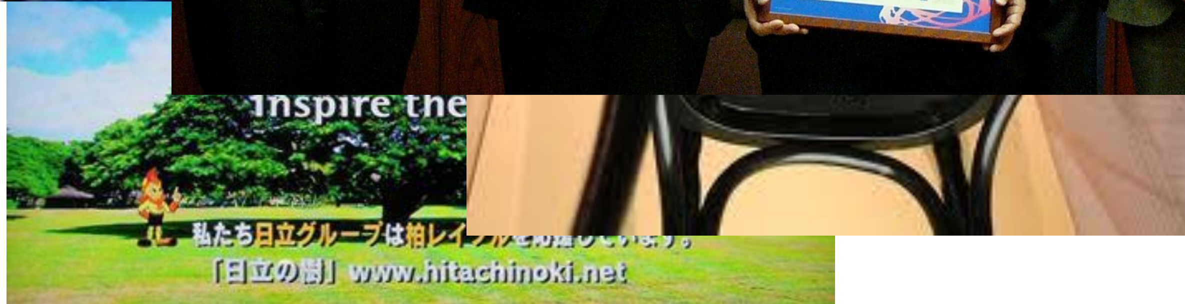

Now, we are benefitting from the company…

Hamamatsu Photonics

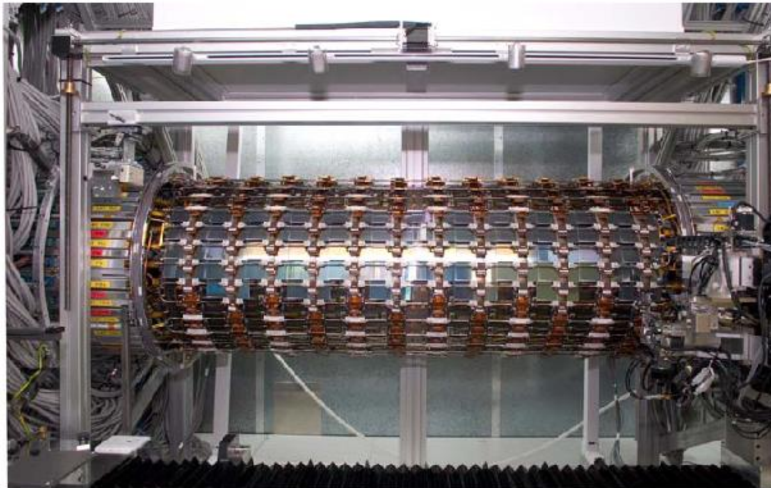

A cylindrical SCT barrel structure, radius 299 mm, length 1492 mm, tiled with rectangular modules constructed using silicon sensors supplied by Hamamatsu Photonics

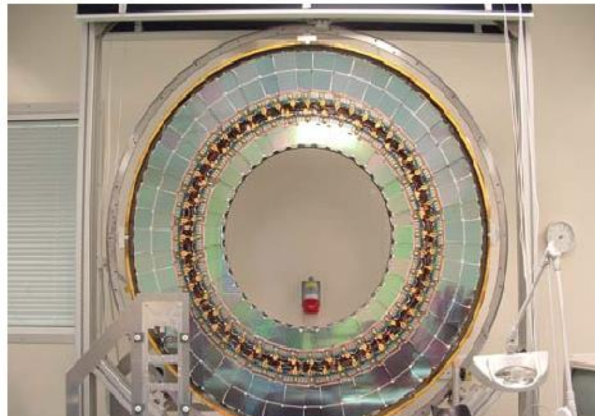

Supply of Silicon Microstrip Sensors for the ATLAS SemiConductor Tracker

Hamamatsu Photonics has supplied 17,028 of the p-in-n single-sided silicon microstrip sensors that make up the detecting element of the ATLAS Semiconductor Tracker. The sensors are of six different shapes, each having 768 ac-coupled readout strips at a pitch close to 80 μm.

The final design details and specifications were developed during several years of collaborative R&D between Hamamatsu Photonics and ATLAS Institutes. The challenge was to produce sensors with high strip quality and efficiency that could withstand the high radiation levels to be experienced in ATLAS, operating at high bias voltages after type-inversion.

The sensors supplied were of uniformly excellent quality, well in excess of the requirements of the technical specification. They were delivered over a three-year period to the agreed schedule and cost. The ATLAS Collaboration greatly appreciates the help, the flexible attitude and the enormous contribution of Hamamatsu Photonics to the experiment.

for the silicon detectors: ATLAS strips ~92%, CMS strips ~97%

rectangular barrel module

with wedge-shaped

Contributions by Japanese teams in the ATLAS construction

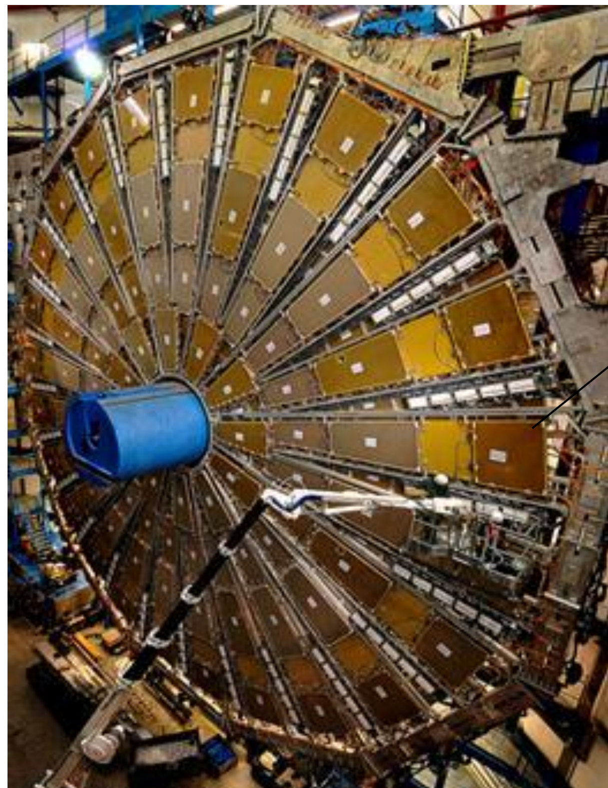

1200 TGC chambers and 320K ch. L1 Electronics of endcap muon trigger system
KEK, Tokyo, Kobe, Nagoya...

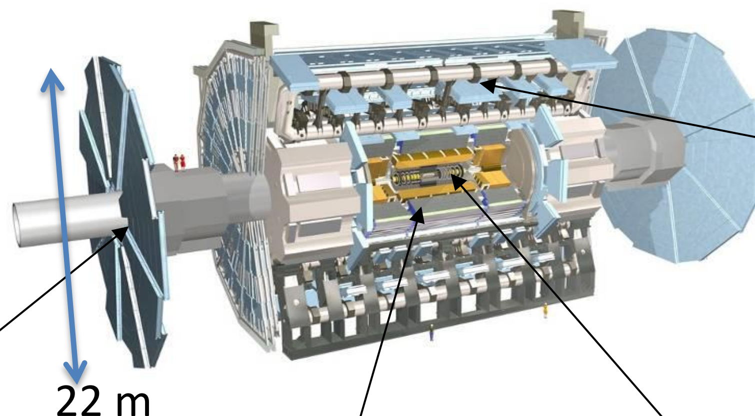

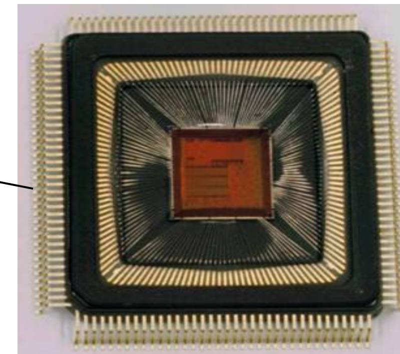

400k ch. of TDC chips for MDT system, KEK

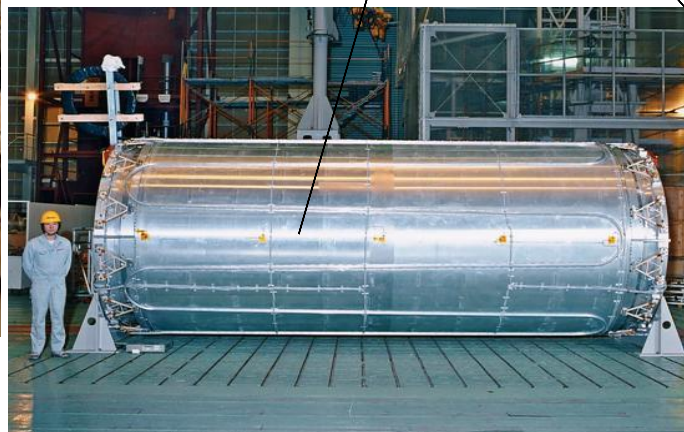

Superconducting Solenoid, KEK

6000 sensors and 980 modules of barrel SCT system, KEK, Tsukuba, Okayama, Hiroshima …

- **In addition, many Japanese industries provided high quality detector components: Hamamatsu Phonics, Kawasaki Heavy Industries, Toshiba, Kuraray, Arisawa, Fujikura, etc**

This lecture

- Micro-strip based detection systems
  – advances and new technological development
- It is not a monopoly of ATLAS nor HPK nor Japan. It is an example of our fields.
  – Other experiments: CMS, LHCb, …
  – Other industries: Microns, CiS, …

- Content
  – Brief overview of the current ATLAS silicon microstrip tracker (SCT)
  – Issues and achievement of the LHC tracker
  – New technological development for the high-luminosity LHC tracker
  – Understanding the underlying physics – TCAD simulation

ATLAS Inner Detector

ID ¼ volume

Solenoid coil
|η|=1.0
|η|=1.5
ID end-plate
3512
Cryostat
PPF1
R1150
712
PPB1
R1066
848
2710
R1004
|η|=2.0
Radius (mm)
TRT (barrel)
TRT (end-cap)
Cryostat
1 2 3 4 5 6 7 8 9 10 11 12 1 2 3 4 5 6 7 8
R644
R563
R560
|η|=2.5
R514
R443
SCT (end-cap)
R438.8
Pixel support tube
R371
SCT (barrel)
R408
R337.6
R299
R275
Pixel PP1
R229
R122.5
R88.5
Pixel
Beam-pipe
R50.5
0
0
400.5
495
580
650
749
853.8
934
1091.5
1299.9
1399.7
1771.4
2115.2
2505
2720.2
z (mm)

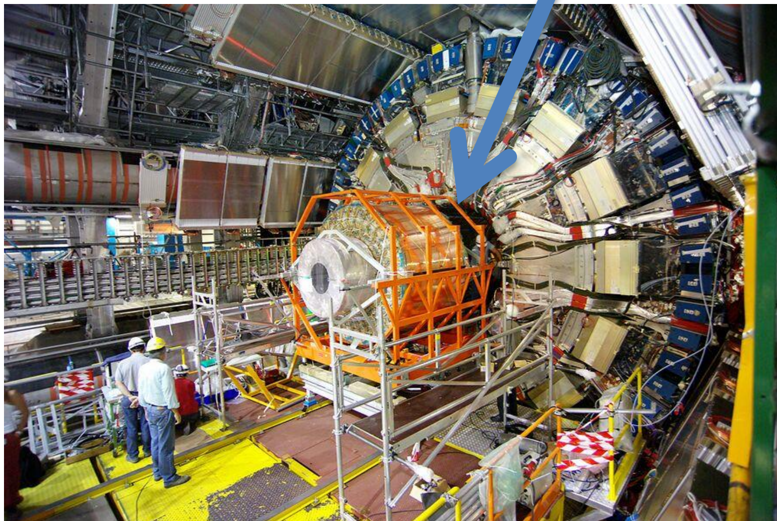

Installation into ATLAS

- ID=Silicon (Pixel + Strip) + TRT
  - Radius~ 1 m, L=5.4 m
- Position (ϕ) resolutions
  - Pixel: ~15 µm (50 µm pitch)
  - Strip (axial-stereo pair): ~17 µm (80 µm pitch)
  - TRT: ~ 22 µm (130 µm drift reso., 36 sampling)
- Why Silicon?

$$dp/p \propto \left[ds/\left(0.3BL^2\right) \right] \times p$$

ATLAS Inner Detector

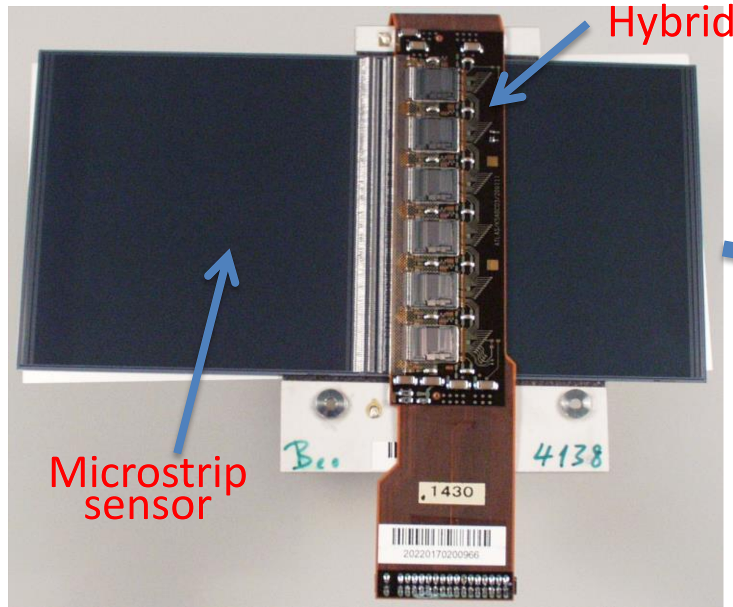

SCT barrel module

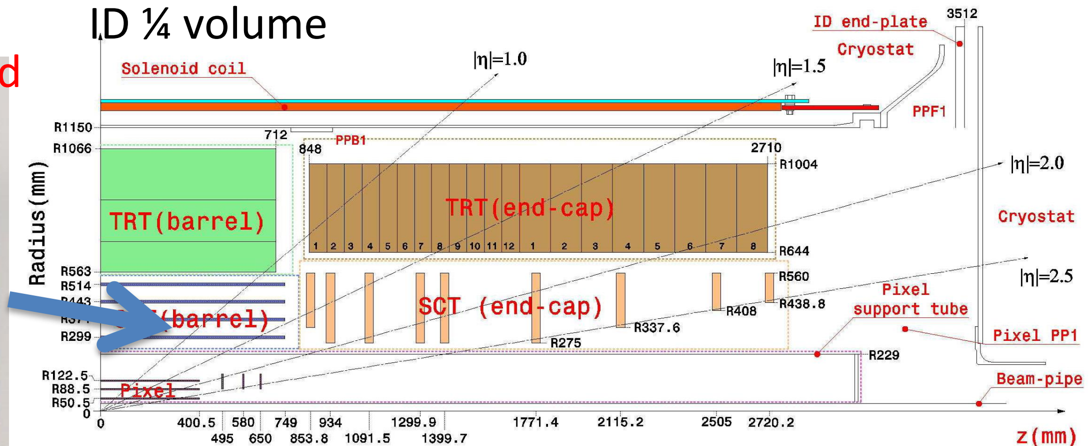

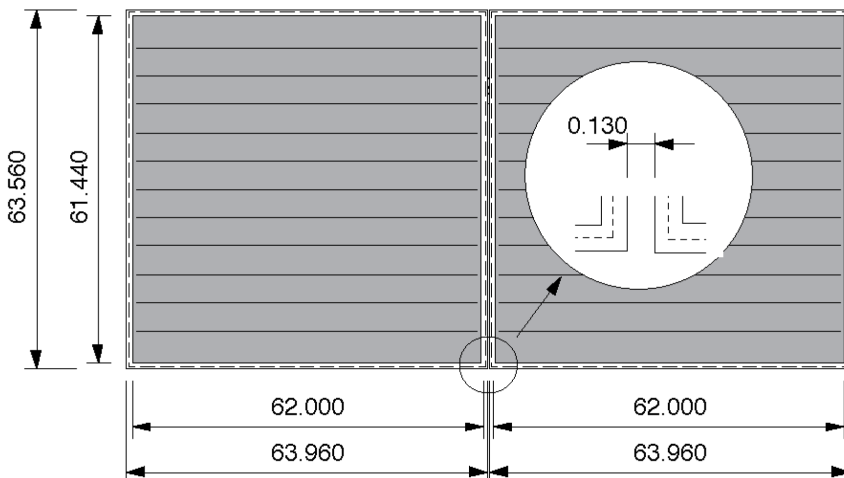

- Barrel modules
  - Double-side, stereo readout (40 mrad)
  - Sensors: 2 x (6.4 x 6.4 cm^2) /side x 2 side (top and bottom)
    - 4 in. FZ crystal wafer, <111> and some <100>
    - 80 μm pitch, ~12.6 cm strip lenth, 768 strips
  - Hybrids: 6 ABCD chips (128 ch)/side
    - Cu/Polyimide flex circuit + Carbon-carbon substrate

Red letters: Contributions of Japan

- Japan: ~980/2112+spares in barrel modules

Silicon Detector (LHC)

Assembly station: aligning two sensors in <5 μm

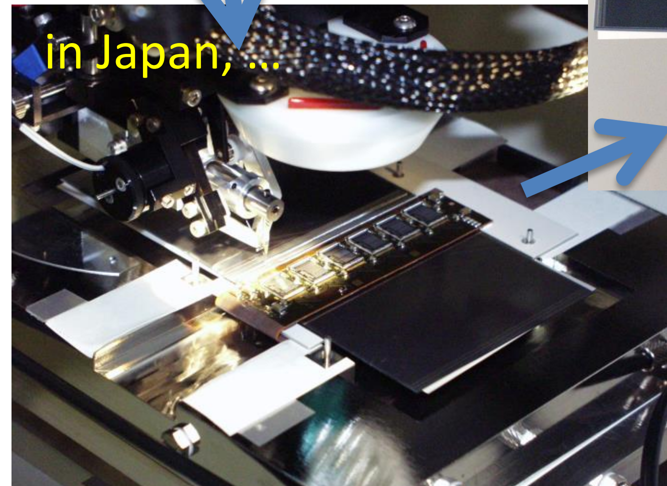

Wire bonding of hybrid-sensor and sensor-sensor: ~3200 bonds

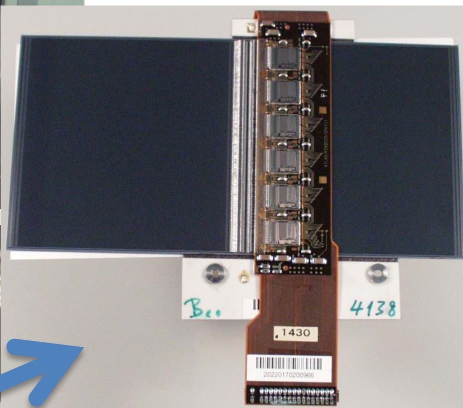

Completed modules

Placement robot

Mounted on the barrel cylinder

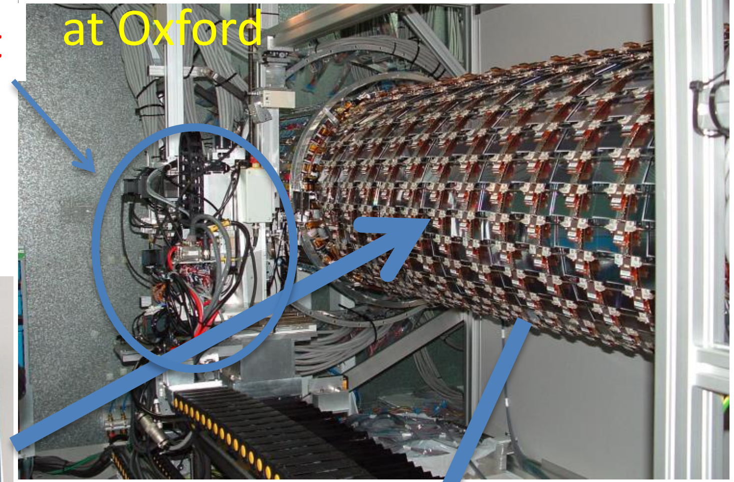

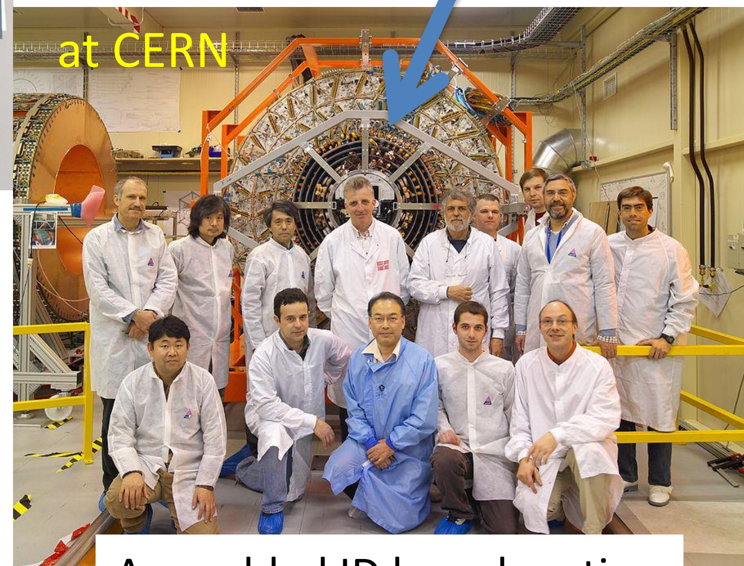

Assembled ID barrel section
Then, installed into ATLAS

Silicon Detector (LHC)

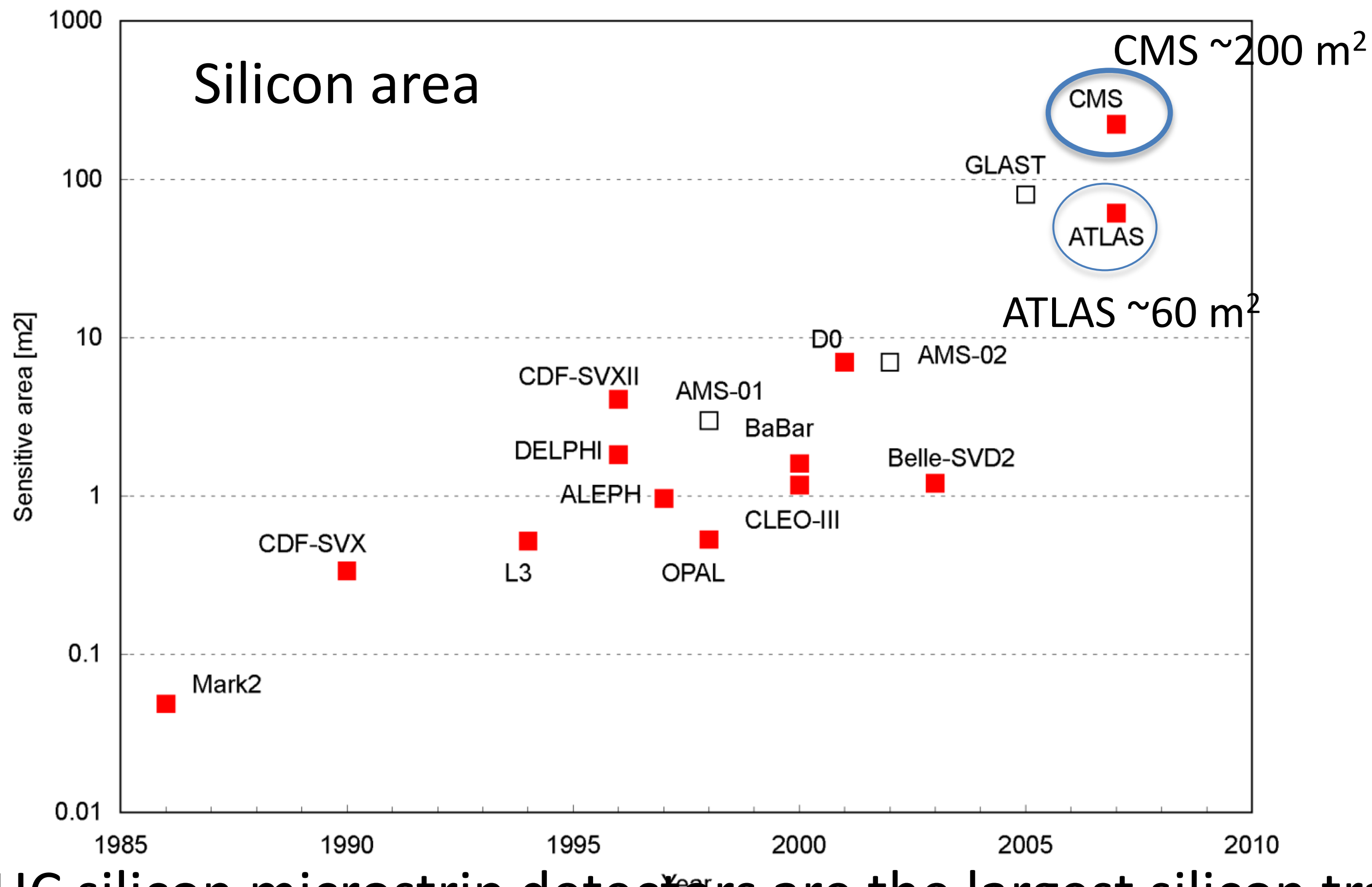

- LHC silicon microstrip detectors are the largest silicon trackers ever built.
  - A scale: cost of the sensor ~1 million Euro/m^2
- Silicon microstrip detector is the "must" for large area coverage.

Particle fluence

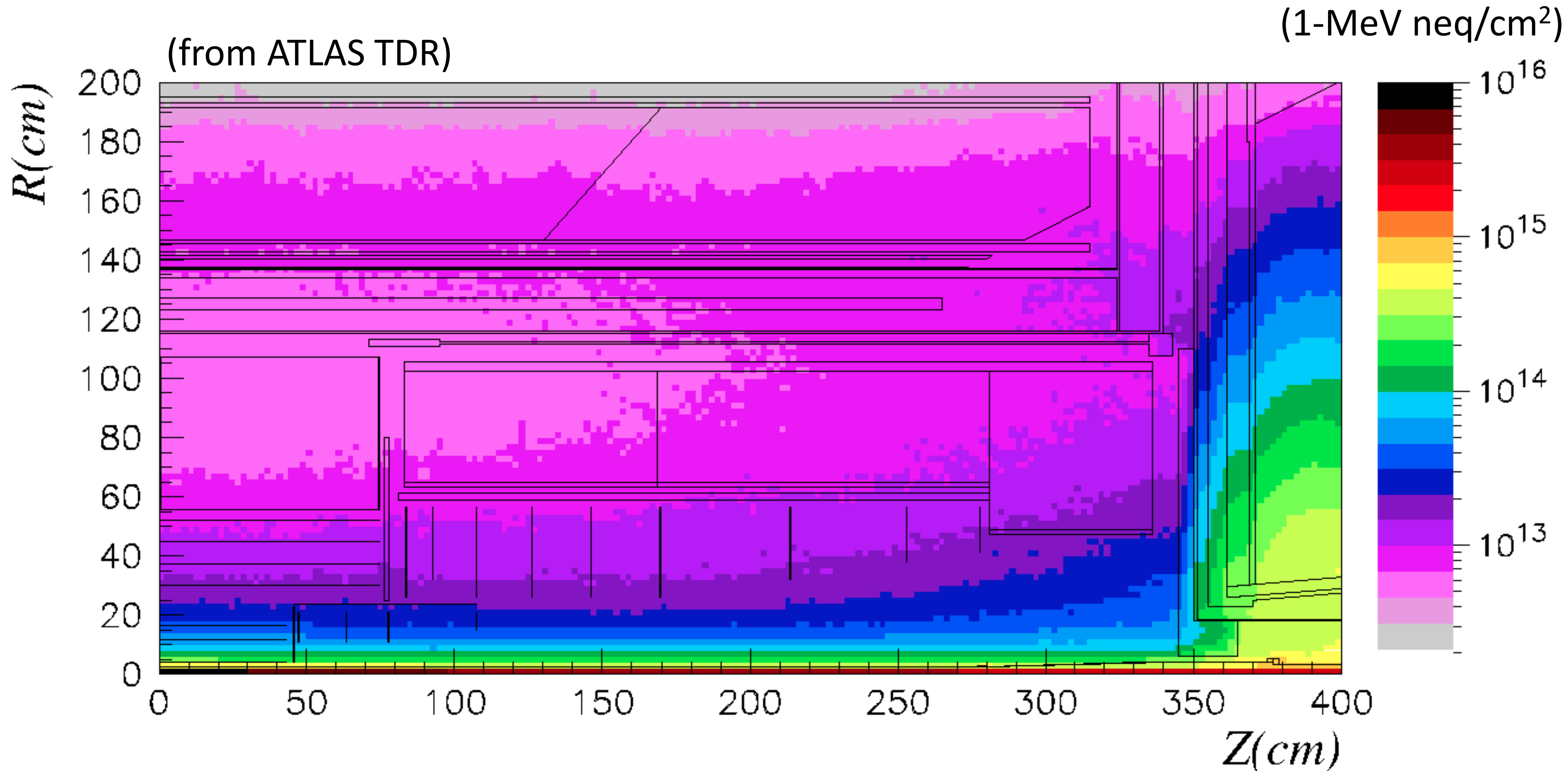

- Yearly fluence of particles
  - in the unit of 1-MeV neutrons equivalent per cm^2
  - Luminosity: 10^{34} $cm^{-2}s^{-1}$, integrated:100 fb^{-1}/yr
- End of life fluence at SCT (r=30 cm)
  - 2×10^{14} 1-MeV neq/cm^2 (including 50% uncertainty in pp cross section)

Non Ionizing Energy Loss (NIEL)

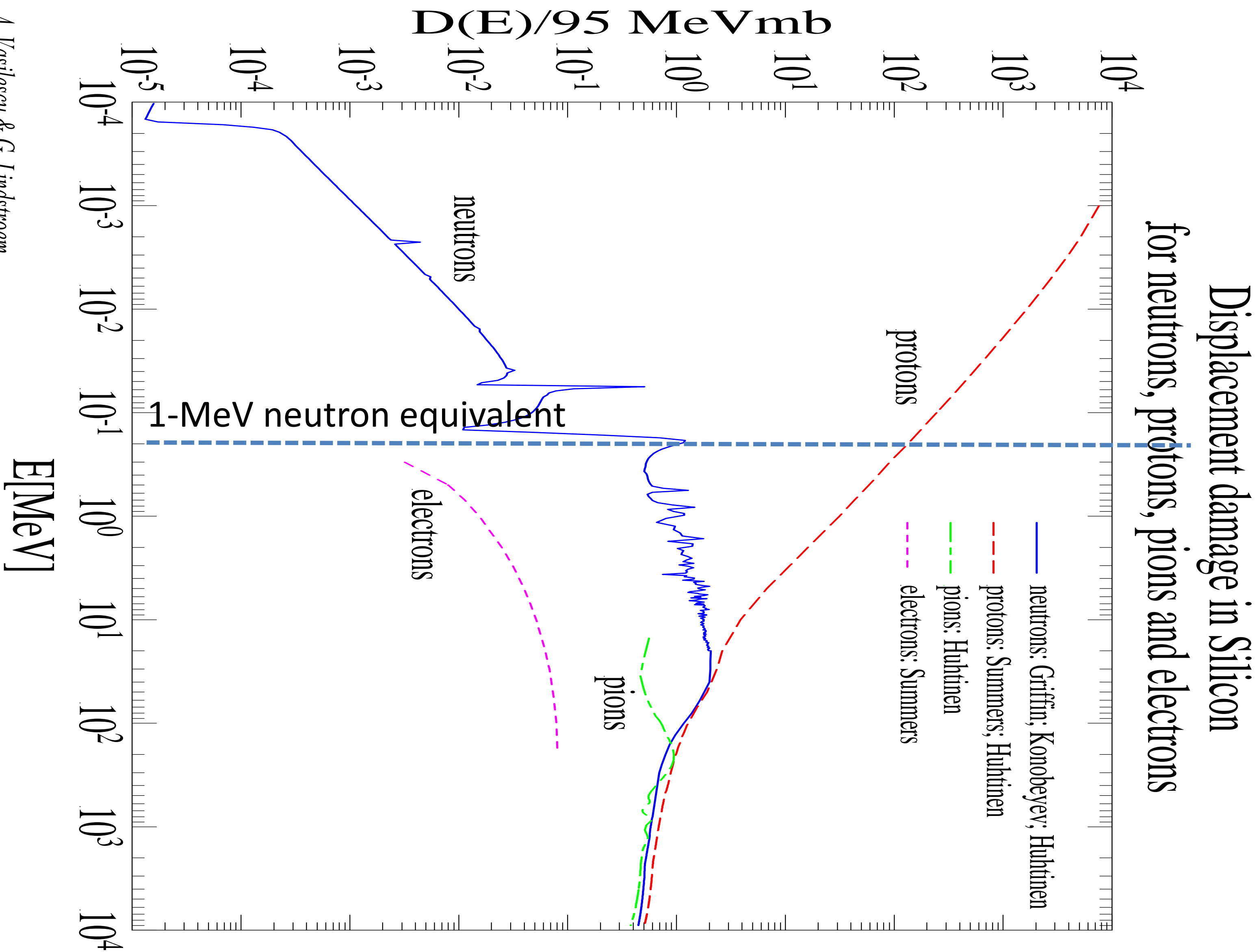

Radiation Damage Studies

- Radiation damage of silicon
  - the 1st, in our field… 30 yrs ago
    - T. Kondo et al, Radiation Damage Test of Silicon Microstrip Detectors
    - Proc. of the 1984 Summer Study on the Design and Utilization of SSC, June 23-July 13, 1984, Snowmass, Colorado, pp. 612-614
- The messages were
  - The prevailing opinion was that silicon vertex detectors were not possible at 10^{33} luminosity, but…
  - It was shown that silicon is rad-hard, little pulse-height change, cooling needed.

Radiation Damage Studies

- Since then, radiation damage studies are continued in Japan, Europe, US., and elsewhere
  - Two papers were already published in 1988, (25 yrs ago)
  - T. Ohsugi, ... T. Kondo, … K. Yamamoto .., “Radiation Damage in Silicon Microstrip DetectorsT”, Nucl. Instr. Meth. A265(1988)105
  - M. Nakamura,…T. Kondo, "Radiation Damage Test of Silicon Multistrip Detectors", Nucl. Instr. Meth. A270(1988)42, using the irradiated sensor by 800 GeV protons

Increase of leakage current

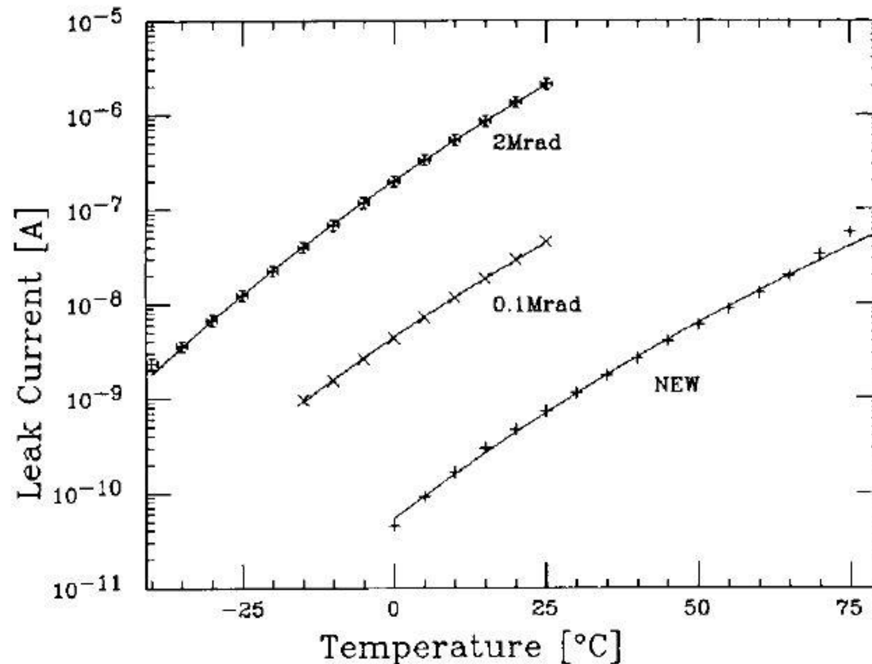

Fig. 5. Temperature dependence of the leakage current. The solid lines are the best fits using the formula given in the text.

Also, temperature dependence of bulk leakage current

$$J_g(T) \propto T^2 \exp(-\frac{E_{ef}}{2k_B T})$$

$$E_{ef} = 1.20\,\mathrm{eV}$$

- Radiation Damage in Silicon Microstrip Detectors
  - T. Ohsugi, ... T. Kondo, … K. Yamamoto .., Nucl. Instr. Meth. A265(1988)105

Type inversion of the silicon

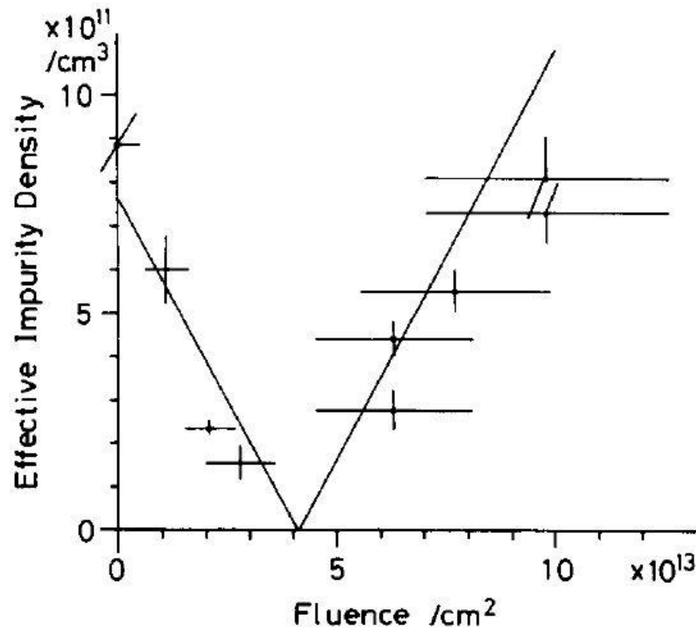

Fig. 25. Estimated effective impurity density as a function of proton fluence.

Abstract:
……. The effective impurity density decreases with fluence up to ~$4x10^{13}/cm^2$, but for greater fluences, it increases. **This may indicate the type conversion** of the bulk silicon ………

- M. Nakamura,…T. Kondo, "Radiation Damage Test of Silicon Multistrip Detectors", Nucl. Instr. Meth. A270(1988)42, using the irradiated sensor by 800 GeV protons

Evolution of depletion voltage

- A thorough study of the radiation damages has been made by RD50 collaboration. But, also done elsewhere…
  - E.g. Michael Moll, Ph.D Thesis, 1999.

24 GeV/c proton irradiation
(n-type silicon)

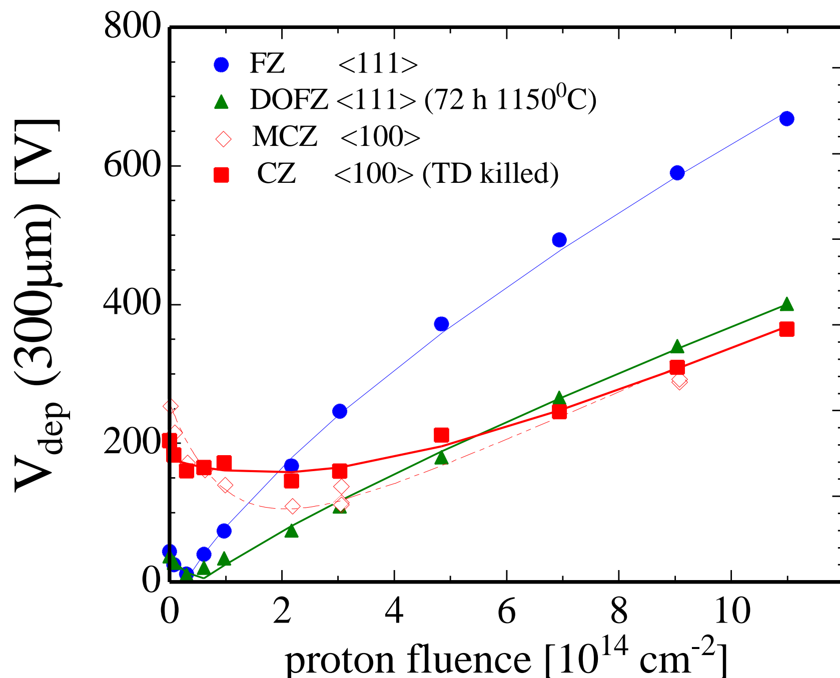

70 MeV proton irradiation
(p-type silicon)

K. Hara et al.,
IEEE Trans. Nucl. Scie. 56 (2009) 468

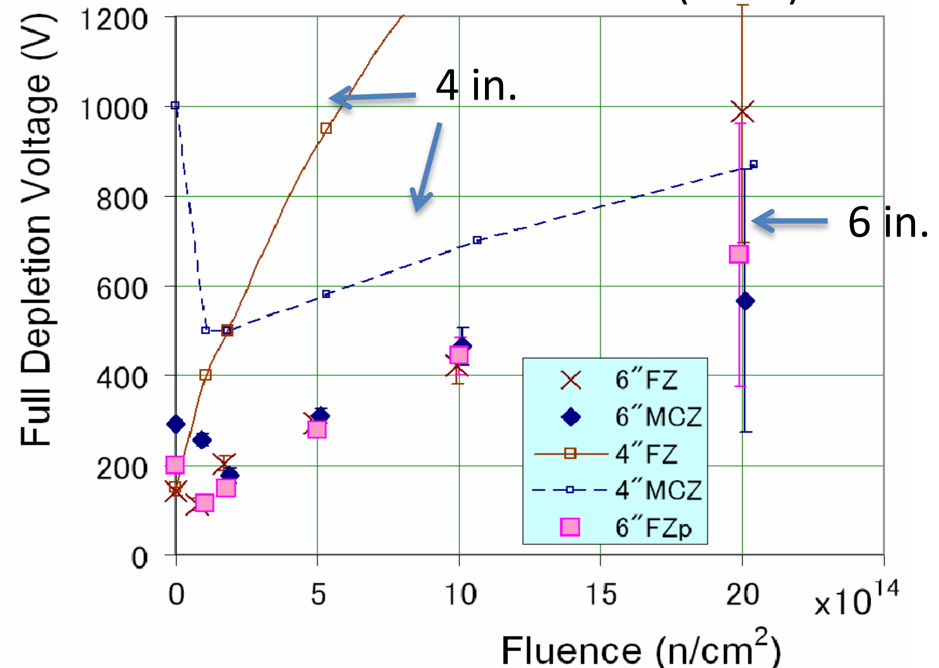

6 in. FZ is as same as DOFZ or MCZ

Signal degradation in LHC Silicon Sensors

Pixel sensors:

max. cumulated fluence for LHC

RD50 collaboration

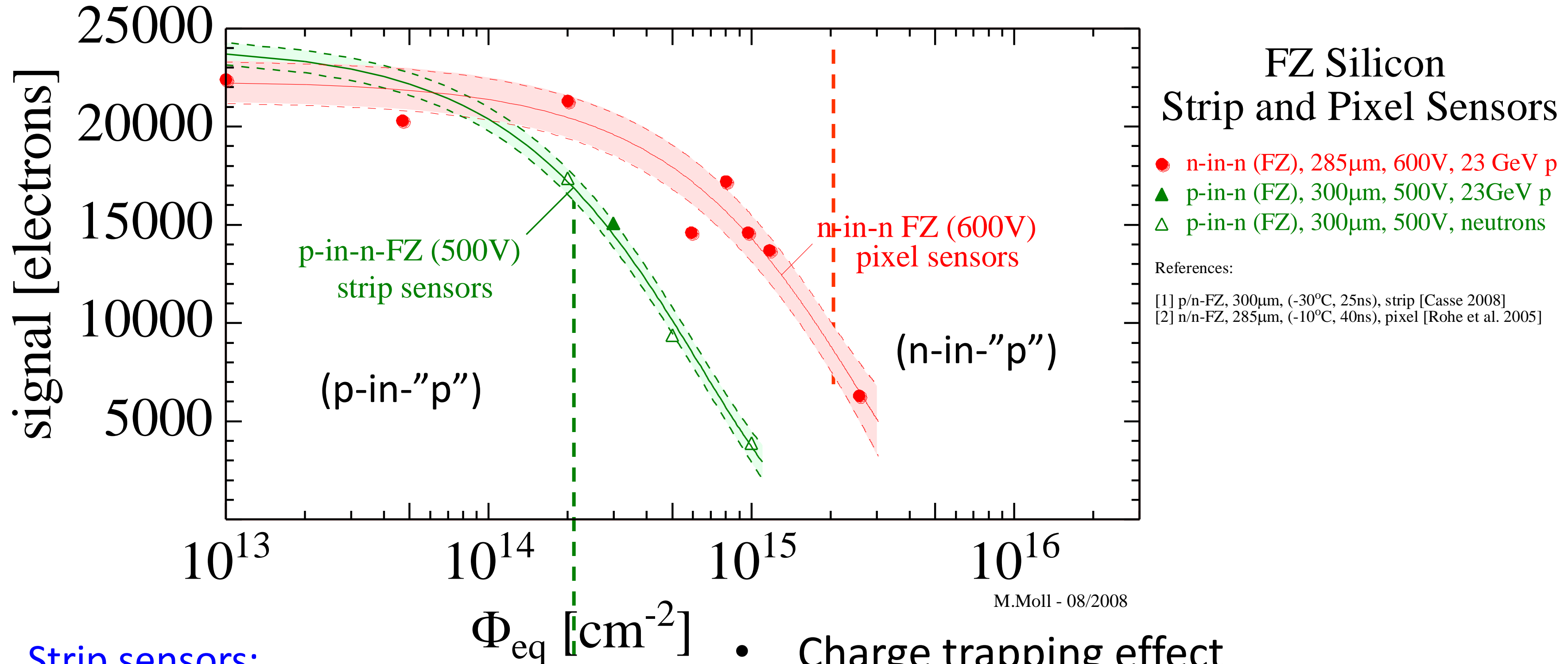

Strip sensors:

max. cumulated fluence for LHC

- Charge trapping effect
  ← Most of signals at around the strips (see Appendix)
- Depleted region
  - p-in-n → p-in-p (requires "full depletion")
  - n-in-n → n-in-p (works under "partial depletion")

Choice of LHC Experiments

Experiment	Type	Wafer
ALICE pixel	p-in-n	standard FZ
ATLAS pixel	n-in-n	oxygenated
ATLAS strips	p-in-n	standard FZ <111> (some <100>)
CMS pixel	n-in-n	standard FZ
CMS strips	p-in-n	standard FZ <100>
LHCb VELO	n-in-n	standard FZ

- Cost consideration and compromises
- p-in-n:
  - single-side process (lower cost)
  - requires full depletion, high voltage operation
- n-in-n
  - double-side process (higher cost)
  - works under partial depletion, less requirement for high voltage

Silicon Detector (LHC ATLAS)

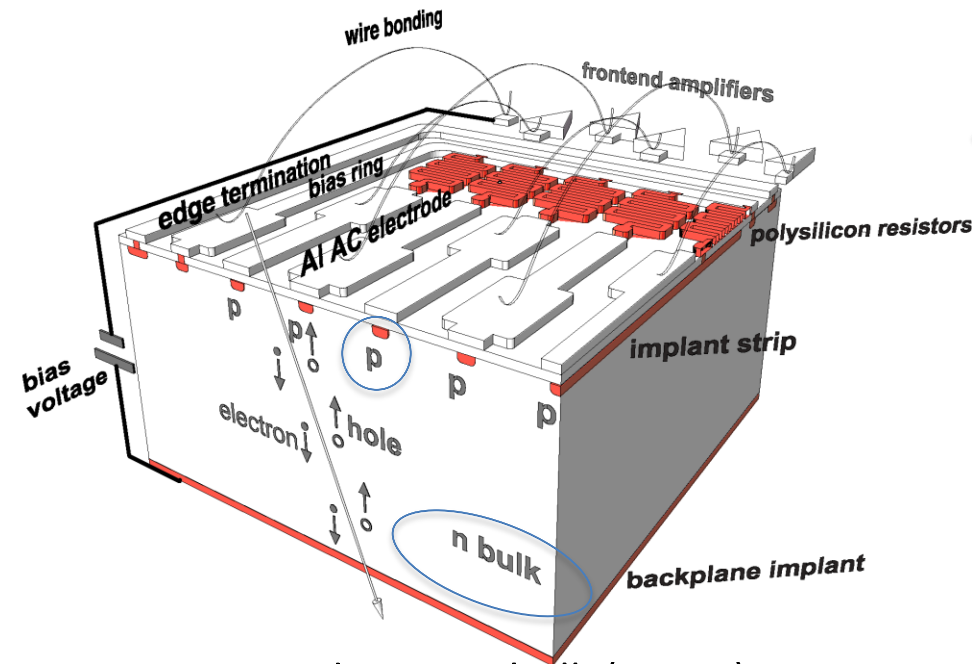

LHC: p-readout in n-bulk (p-in-n)

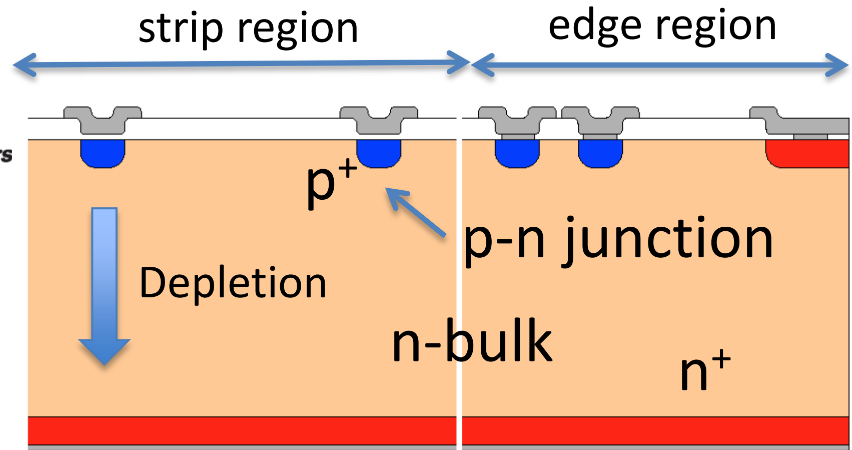

after type-inversion

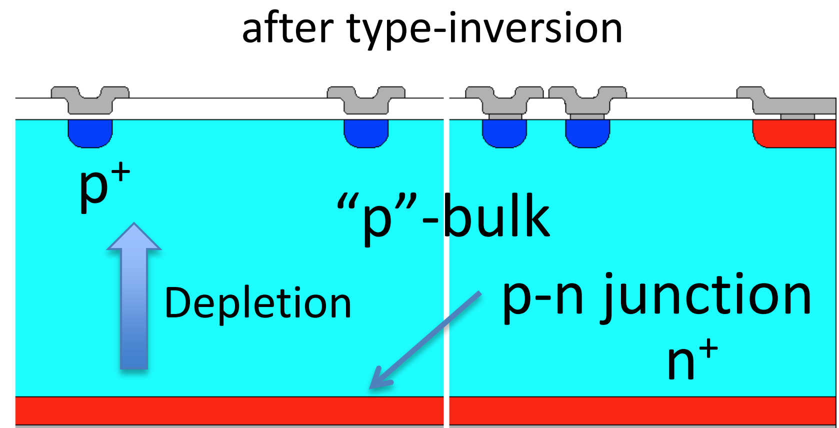

- Silicon sensor principle
  - Deplete the bulk by holding the bias voltage at p-n junction
- LHC ATLAS: p-in-n strip sensor
  - N-bulk: conventional
  - Cheaper than other options
  - Need full depletion
    - 500 V max operation/specification

Radiation damage – Surface effect

S.M. Sze, Physics of Semiconductor Devices, 2nd ed., p380

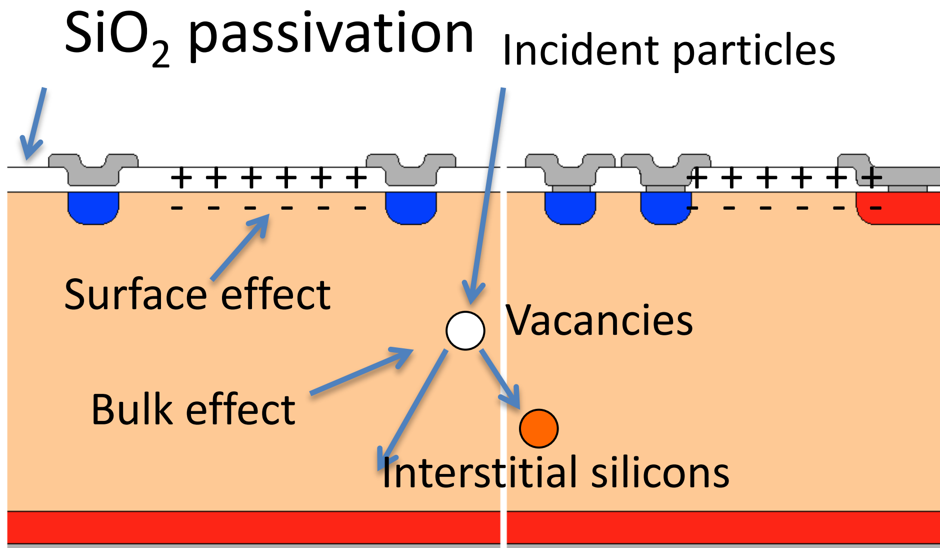

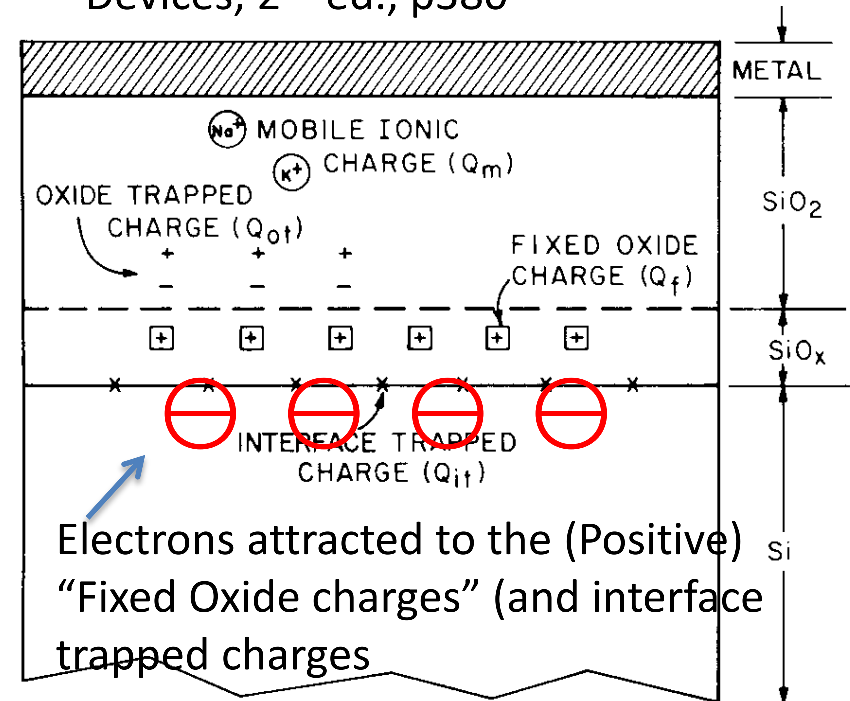

- The interfacial region is a single-crystal silicon followed by a monolayer of SiO_x, incompletely oxidized silicon, then a strained region of SiO_2 roughly 10-40 A deep.
- Interface traps (Q_{if}) and fixed oxide charges (Q_f) exist, (as a consequence of thermal oxidation)
- Oxide trapped charges (Q_{ot}) can be created by radiation.
- Q_f and Q_{ot} are "positve" and attract electrons in the Si-SiO_2 interface.

1st Visualization of Microdischarge

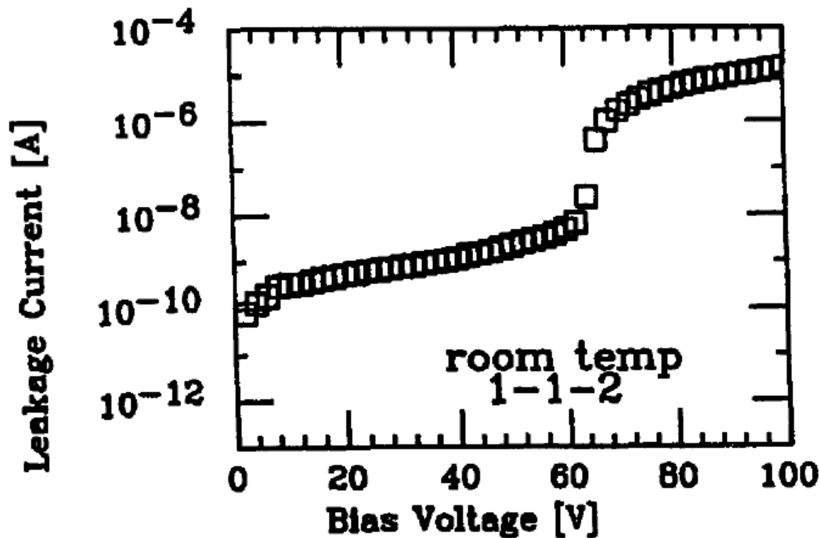

Fig. 1. Leakage current as a function of the bias voltage when the potential is across the integrated capacitor on the p-strip.

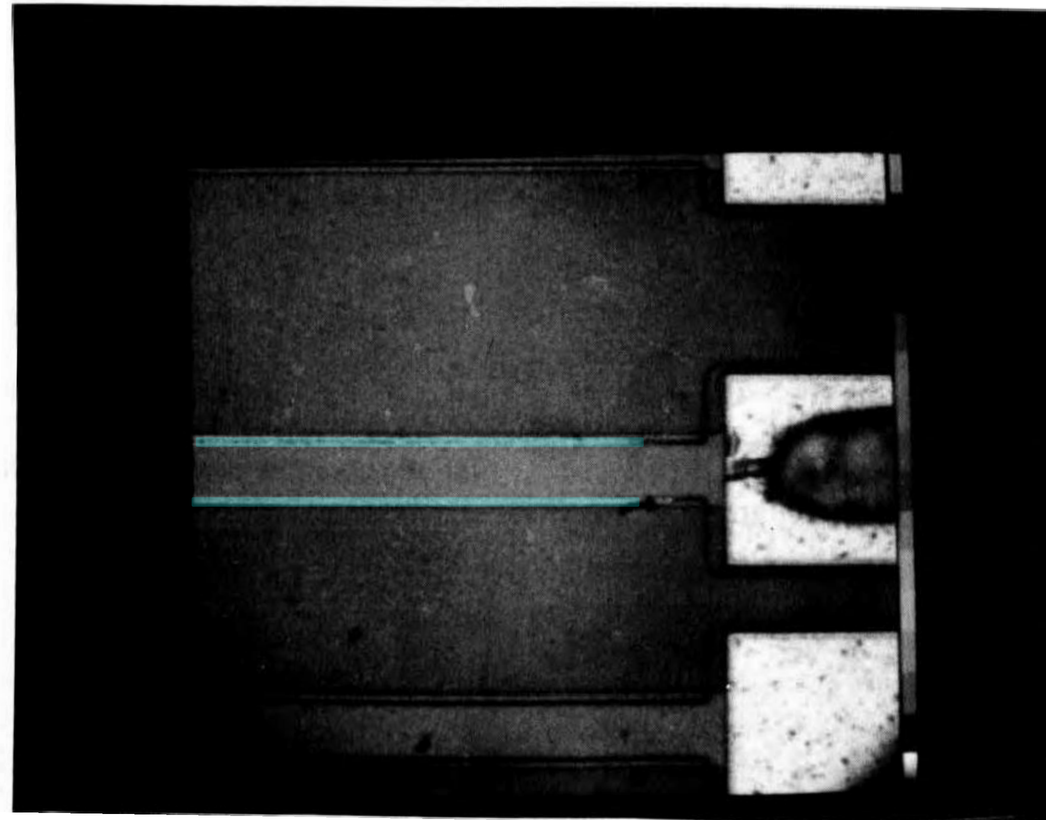

- High bias voltage → High electric field → avalanche breakdown
  - *Breakdown field* ~ 30 V/μm in silicon
- Visualization with an infra-red sensitive camera
- T. Ohsugi et al., Nucl. Instr. Meth. A432 (1994) 22

Other examples of hot spots

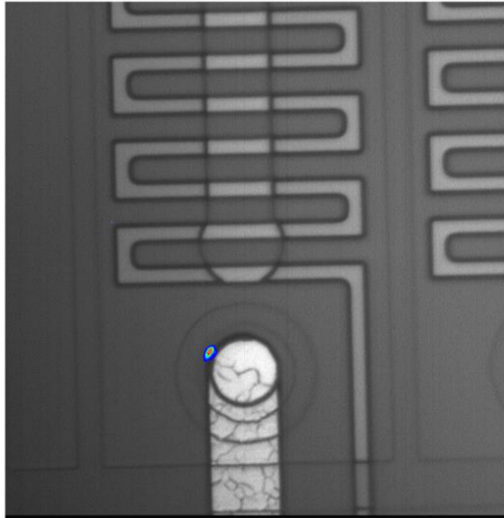

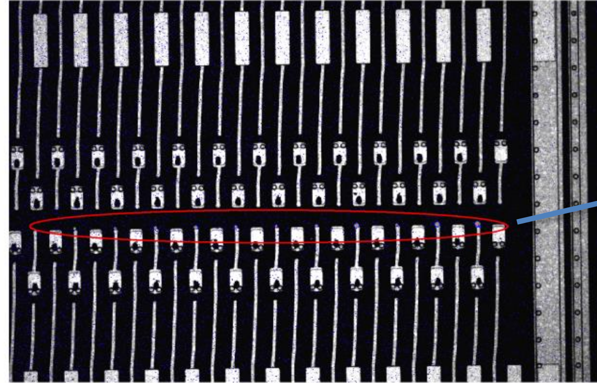

Seg4 の DC PAD ｽﾄﾗｲﾌﾟ 先端で発光（×5）

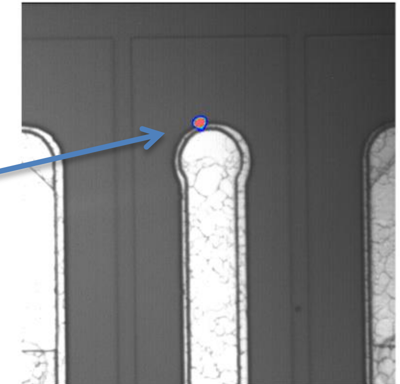

Seg4 の DC PAD ｽﾄﾗｲﾌﾟ 先端で発光（×100）

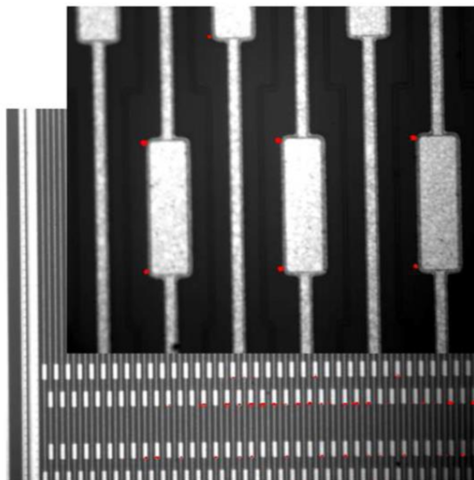

Fig. 9. Hot spots observed at AC pad corners. The AC pad is 60 μm wide and 200 μm long.

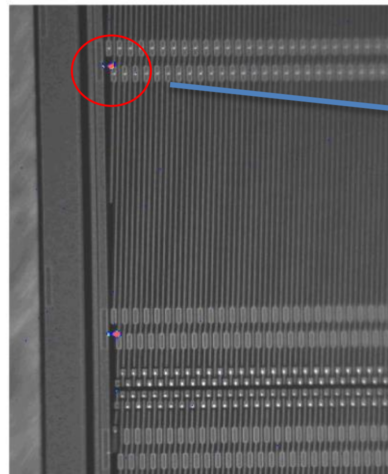

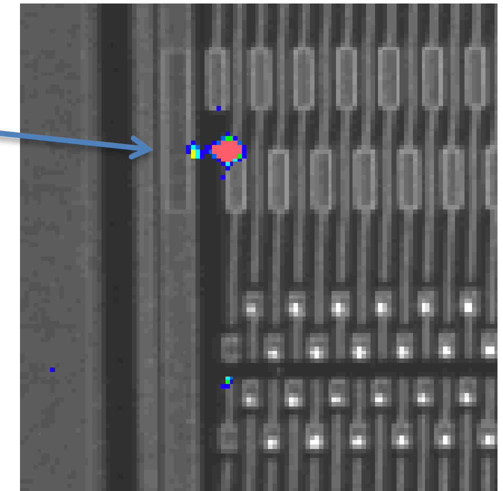

の AC PAD 角と Seg4 の DC PAD ｽﾄﾗｲﾌﾟ 先端で発光（×0.8）

Y. Unno et al., Nucl. Instr. Meth. A Supplement 636 (2011) S24

Y. Takahasi et al., http://dx.doi.org/10.1016/j.nima.2012.04.031

Microdischarge after Irradiation

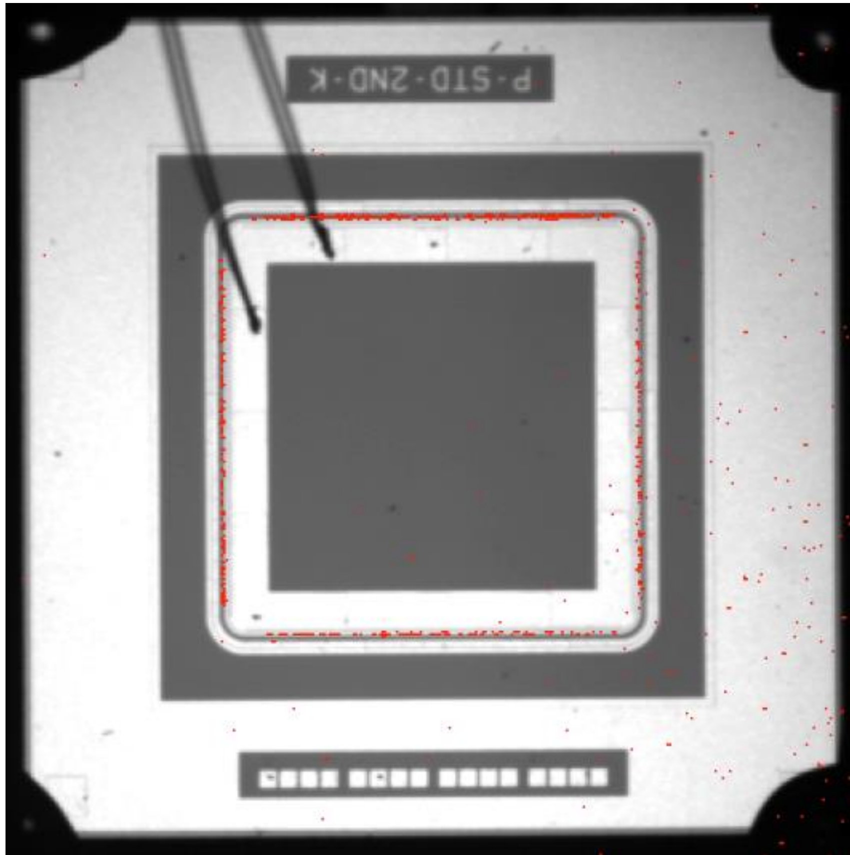

CYRIC proton irradiated
$1\text{x}10^{14}\ n_{eq}/\text{cm}^2$
10 uA at 2000 V
-15 ° C

S. Mitsui et al.,
Nucl. Instr. Meth. A699 (2013) 36-40

- Hot electron images confirm that
  - hot spots were observed first at the edge of the bias ring, and then at the inside of the edge metal.
  - the highest electric field is at the bias ring (n^+ implant), not at the edge ring (p^+ implant).

Design of the sensor to high bias voltage

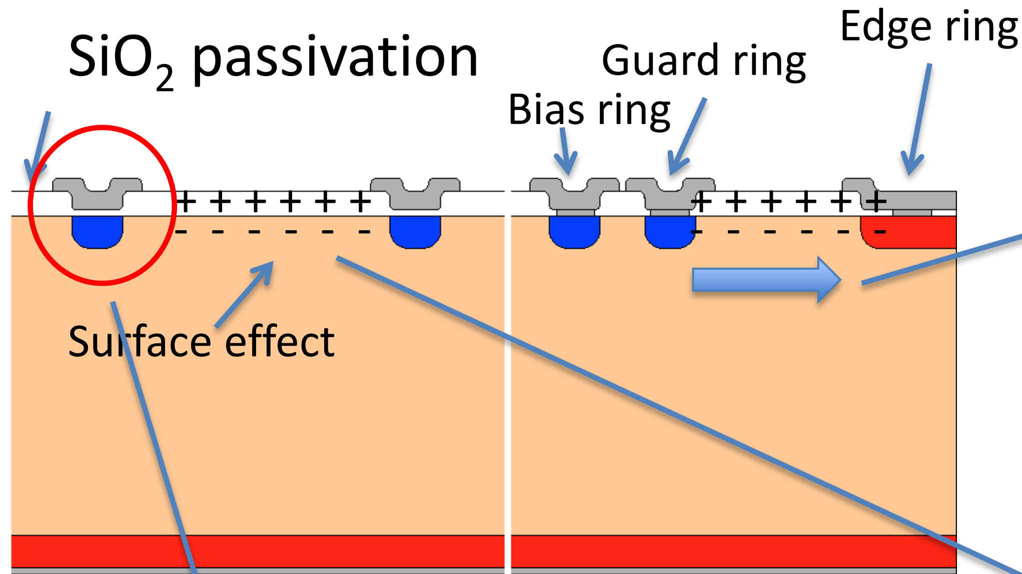

②

Optimize the edge structure
→ Width, guard ring between the bias and the dicing edge

HPK design:

1) width ~ 1 mm
2) minimum # guard rings, i.e. 1

①

Move the highest electric field from Si (to SiO_2)
→ Extended electronde

Under the condition of

1) Same potential in implant and metal

③

Reduce the oxide fixed/trap charges
→ <100> crystal orientation

Less "dangling" bonds in interface

<100>: $\sim 10^{10}$ ions/cm^2

<111>: $\sim 10^{11}$ ions/cm^2

⓪

Clean and high quality process
→ little irregularity at high field where HPK is appreciated.

ATLAS SCT in operation

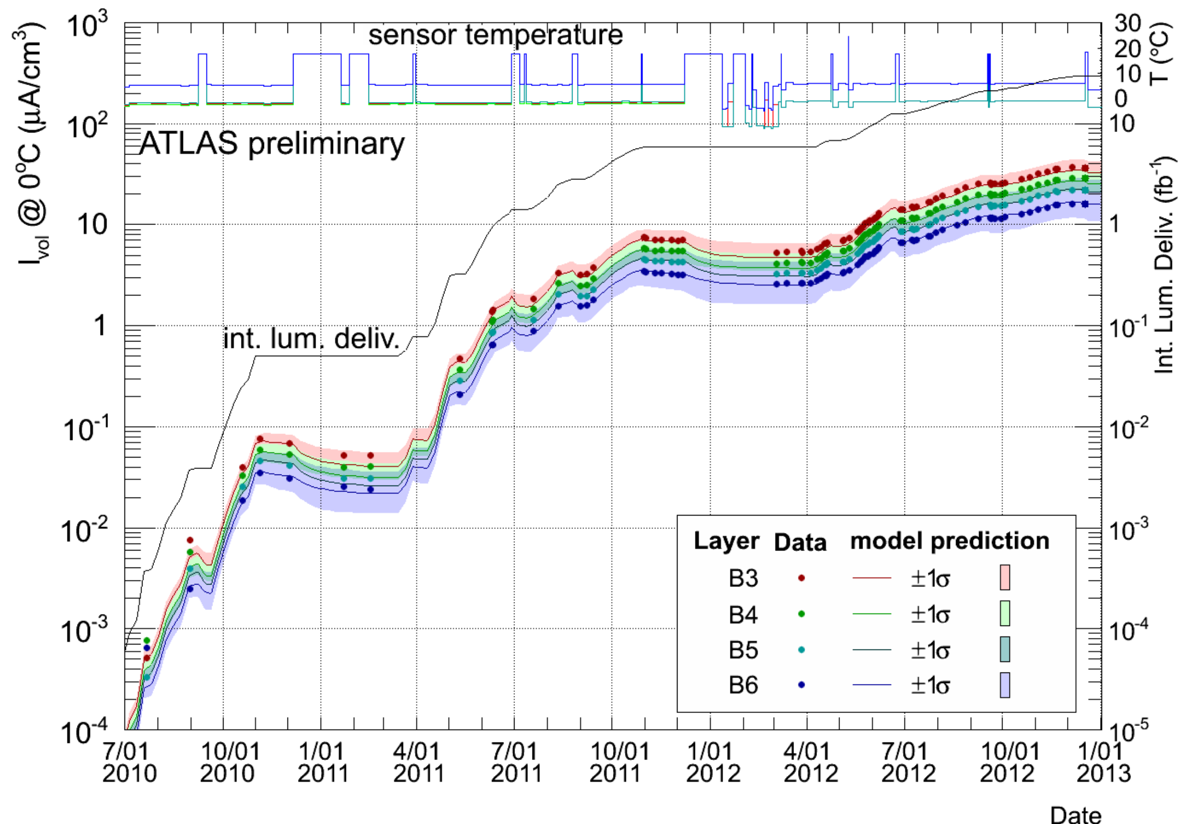

- Radiation damage monitoring
  - Leakage currents are well consistent with the expectation
- 99.3% modules are working
  - 30/4088 modules were disabled due to LV, HV, Cooling problems, …

LHC Upgrade (HL-LHC)

Higgs search

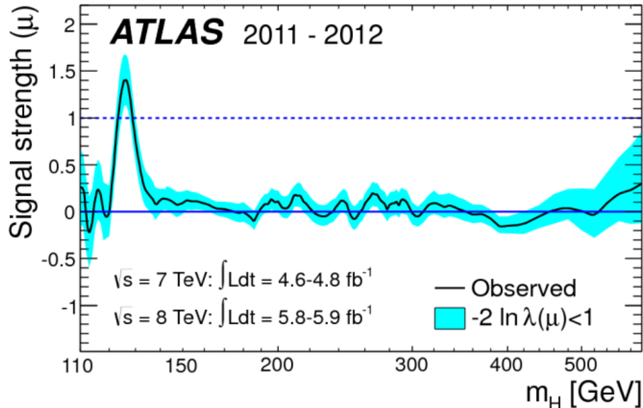

Phys. Lett. B 716 (2012) 1-29 Fig.7c

ATLAS SUSY Searches* - 95% CL Lower Limits

Status: LP 2013

ATLAS Preliminary

$\int \mathcal{L} dt = (4.4 - 22.9)\ \mathrm{fb}^{-1}$ $\sqrt{s} = 7, 8$ TeV

	Model	e, μ, τ, γ	Jets	E_T^{miss}	$\int \mathcal{L} dt[\mathrm{fb}^{-1}]$	Mass limit		Reference
Inclusive Searches	MSUGRA/CMSSM	1 e,μ	3-6 jets	Yes	20.3	$\tilde{g}$ 1.2 TeV	any $m(\tilde{q})$	ATLAS-CONF-2013-062
	MSUGRA/CMSSM	0	7-10 jets	Yes	20.3	$\tilde{g}$ 1.1 TeV	any $m(\tilde{q})$	ATLAS-CONF-2013-054
	$\tilde{q}\tilde{q}, \tilde{q}\to q\tilde{\chi}_1^0$	0	2-6 jets	Yes	20.3	$\tilde{q}$ 740 GeV	$m(\tilde{\chi}_1^0)$=0 GeV	ATLAS-CONF-2013-047
	$\tilde{g}\tilde{g}, \tilde{g}\to q\bar{q}\tilde{\chi}_1^0$	0	2-6 jets	Yes	20.3	$\tilde{g}$ 1.3 TeV	$m(\tilde{\chi}_1^0)$=0 GeV	ATLAS-CONF-2013-047
	$\tilde{g}\tilde{g}, \tilde{g}\to qq\tilde{\chi}_1^\pm \to qqW^\pm\tilde{\chi}_1^0$	1 e,μ	3-6 jets	Yes	20.3	$\tilde{g}$ 1.18 TeV	$m(\tilde{\chi}_1^0)$<200 GeV, $m(\tilde{\chi}^\pm)$=0.5($m(\tilde{\chi}_1^0)$+$m(\tilde{g})$)	ATLAS-CONF-2013-062
	$\tilde{g}\tilde{g}\to qqqq\ell\ell(\ell\ell)\tilde{\chi}_1^0\tilde{\chi}_1^0$	2 e,μ (SS)	3 jets	Yes	20.7	$\tilde{g}$ 1.1 TeV	$m(\tilde{\chi}_1^0)$<650 GeV	ATLAS-CONF-2013-007
	GMSB ($\tilde{\ell}$ NLSP)	2 e,μ	2-4 jets	Yes	4.7	$\tilde{g}$ 1.24 TeV	$\tan\beta$<15	1208.4688
	GMSB ($\tilde{\ell}$ NLSP)	1-2 τ	0-2 jets	Yes	20.7	$\tilde{g}$ 1.4 TeV	$\tan\beta$>18	ATLAS-CONF-2013-026
	GGM (bino NLSP)	2 γ	0	Yes	4.8	$\tilde{g}$ 1.07 TeV	$m(\tilde{\chi}_1^0)$>50 GeV	1209.0753
	GGM (wino NLSP)	1 $e,\mu+\gamma$	0	Yes	4.8	$\tilde{g}$ 619 GeV	$m(\tilde{\chi}_1^0)$>50 GeV	ATLAS-CONF-2012-144
	GGM (higgsino-bino NLSP)	γ	1 b	Yes	4.8	$\tilde{g}$ 900 GeV	$m(\tilde{\chi}_1^0)$>220 GeV	1211.1167
	GGM (higgsino NLSP)	2 e,μ (Z)	0-3 jets	Yes	5.8	$\tilde{g}$ 690 GeV	$m(\tilde{H})$>200 GeV	ATLAS-CONF-2012-152
	Gravitino LSP	0	mono-jet	Yes	10.5	$F^{1/2}$ scale 645 GeV	$m(\tilde{g})>10^{-4}$ eV	ATLAS-CONF-2012-147
3rd gen. $\tilde{g}$ med.	$\tilde{g}\to b\bar{b}\tilde{\chi}_1^0$	0	3 b	Yes	20.1	$\tilde{g}$ 1.2 TeV	$m(\tilde{\chi}_1^0)$<600 GeV	ATLAS-CONF-2013-061
	$\tilde{g}\to t\bar{t}\tilde{\chi}_1^0$	0	7-10 jets	Yes	20.3	$\tilde{g}$ 1.14 TeV	$m(\tilde{\chi}_1^0)$ <200 GeV	ATLAS-CONF-2013-054
	$\tilde{g}\to t\bar{t}\tilde{\chi}_1^0$	0-1 e,μ	3 b	Yes	20.1	$\tilde{g}$ 1.34 TeV	$m(\tilde{\chi}_1^0)$<400 GeV	ATLAS-CONF-2013-061
	$\tilde{g}\to b\bar{t}\tilde{\chi}_1^+$	0-1 e,μ	3 b	Yes	20.1	$\tilde{g}$ 1.3 TeV	$m(\tilde{\chi}_1^0)$<300 GeV	ATLAS-CONF-2013-061
3rd gen. squarks direct production	$\tilde{b}_1\tilde{b}_1, \tilde{b}_1\to b\tilde{\chi}_1^0$	0	2 b	Yes	20.1	$\tilde{b}_1$ 100-630 GeV	$m(\tilde{\chi}_1^0)$<100 GeV	ATLAS-CONF-2013-053
	$\tilde{b}_1\tilde{b}_1, \tilde{b}_1\to t\tilde{\chi}_1^\pm$	2 e,μ (SS)	0-3 b	Yes	20.7	$\tilde{b}_1$ 430 GeV	$m(\tilde{\chi}_1^\pm)$=2 $m(\tilde{\chi}_1^0)$	ATLAS-CONF-2013-007
	$\tilde{t}_1\tilde{t}_1$(light), $\tilde{t}_1\to b\tilde{\chi}_1^\pm$	1-2 e,μ	1-2 b	Yes	4.7	$\tilde{t}_1$ 167 GeV	$m(\tilde{\chi}_1^0)$=55 GeV	1208.4305, 1209.2102
	$\tilde{t}_1\tilde{t}_1$(light), $\tilde{t}_1\to Wb\tilde{\chi}_1^0$	2 e,μ	0-2 jets	Yes	20.3	$\tilde{t}_1$ 220 GeV	$m(\tilde{\chi}_1^0)$ =$m(\tilde{t}_1)$-$m(W)$-50 GeV, $m(\tilde{t}_1)$<<$m(\tilde{\chi}_1^\pm)$	ATLAS-CONF-2013-048
	$\tilde{t}_1\tilde{t}_1$(medium), $\tilde{t}_1\to b\tilde{\chi}_1^\pm$	2 e,μ	0-2 jets	Yes	20.3	$\tilde{t}_1$ 150-440 GeV	$m(\tilde{\chi}_1^0)$=0 GeV, $m(\tilde{t}_1)$-$m(\tilde{\chi}_1^\pm)$=10 GeV	ATLAS-CONF-2013-048
	$\tilde{t}_1\tilde{t}_1$(medium), $\tilde{t}_1\to b\tilde{\chi}_1^\pm$	0	2 b	Yes	20.1	$\tilde{t}_1$ 150-580 GeV	$m(\tilde{\chi}_1^0)$<200 GeV, $m(\tilde{\chi}_1^\pm)$-$m(\tilde{\chi}_1^0)$=5 GeV	ATLAS-CONF-2013-053
	$\tilde{t}_1\tilde{t}_1$(heavy), $\tilde{t}_1\to t\tilde{\chi}_1^0$	1 e,μ	1 b	Yes	20.7	$\tilde{t}_1$ 200-610 GeV	$m(\tilde{\chi}_1^0)$=0 GeV	ATLAS-CONF-2013-037
	$\tilde{t}_1\tilde{t}_1$(heavy), $\tilde{t}_1\to t\tilde{\chi}_1^0$	0	2 b	Yes	20.5	$\tilde{t}_1$ 320-660 GeV	$m(\tilde{\chi}_1^0)$=0 GeV	ATLAS-CONF-2013-024
	$\tilde{t}_1\tilde{t}_1$(natural GMSB)	2 e,μ (Z)	1 b	Yes	20.7	$\tilde{t}_1$ 500 GeV	$m(\tilde{\chi}_1^0)$>150 GeV	ATLAS-CONF-2013-025
	$\tilde{t}_2\tilde{t}_2, \tilde{t}_2\to\tilde{t}_1+Z$	3 e,μ (Z)	1 b	Yes	20.7	$\tilde{t}_2$ 520 GeV	$m(\tilde{t}_1)$=$m(\tilde{\chi}_1^0)$+180 GeV	ATLAS-CONF-2013-025
	$\tilde{\ell}_{L,R}\tilde{\ell}_{L,R}, \tilde{\ell}\to\ell\tilde{\chi}_1^0$	2 e,μ	0	Yes	20.3	$\tilde{\ell}$ 85-315 GeV	$m(\tilde{\chi}_1^0)$=0 GeV	ATLAS-CONF-2013-049
						125-450 GeV	$m(\tilde{\chi}_1^0)$=0 GeV, $m(\tilde{\ell},\tilde{\nu})$=0.5($m(\tilde{\chi}_1^\pm)$+$m(\tilde{\chi}_1^0)$)	ATLAS-CONF-2013-049
						180-330 GeV	$m(\tilde{\chi}_1^0)$=0 GeV, $m(\tilde{\tau},\tilde{\nu})$=0.5($m(\tilde{\chi}_1^\pm)$+$m(\tilde{\chi}_1^0)$)	ATLAS-CONF-2013-028
						600 GeV	$m(\tilde{\chi}_1^\pm)$=$m(\tilde{\chi}_2^0)$, $m(\tilde{\chi}_1^0)$=0, $m(\tilde{\ell},\tilde{\nu})$=0.5($m(\tilde{\chi}_1^\pm)$+$m(\tilde{\chi}_1^0)$)	ATLAS-CONF-2013-035
						315 GeV	$m(\tilde{\chi}_1^\pm)$=$m(\tilde{\chi}_2^0)$, $m(\tilde{\chi}_1^0)$=0, sleptons decoupled	ATLAS-CONF-2013-035
						220 GeV	1<$\tau(\tilde{\chi}_1^\pm)$<10 ns	1210.2852
						857 GeV	$m(\tilde{\chi}_1^0)$=100 GeV, 10 μs<$\tau(\tilde{g})$<1000 s	ATLAS-CONF-2013-057
						385 GeV	5<$\tan\beta$<50	ATLAS-CONF-2013-058
						395 GeV	$m(\tilde{\tau})$=$m(\tilde{\ell})$	ATLAS-CONF-2013-058
						230 GeV	0.4<$\tau(\tilde{\chi}_1^0)$<2 ns	1304.6310
						700 GeV	1 mm<$c\tau$<1 m, $\tilde{g}$ decoupled	1210.7451
						1.61 TeV	λ'_{311}=0.10, λ_{132}=0.05	1212.1272
						1.1 TeV	λ'_{311}=0.10, $\lambda_{1(2)33}$=0.05	1212.1272
						1.2 TeV	$m(\tilde{q})$=$m(\tilde{g})$, $c\tau_{LSP}$<1 mm	ATLAS-CONF-2012-140
						760 GeV	$m(\tilde{\chi}_1^0)$>300 GeV, λ_{121}>0	ATLAS-CONF-2013-036
						350 GeV	$m(\tilde{\chi}_1^0)$>80 GeV, λ_{133}>0	ATLAS-CONF-2013-036
						666 GeV		1210.4813
						880 GeV		ATLAS-CONF-2013-007
						100-287 GeV	incl. limit from 1110.2693	1210.4826
						704 GeV	$m(\chi)$<80 GeV, limit of<687 GeV for D8	ATLAS-CONF-2012-147

Mass scale [TeV] (10^{-1}, 1)

1 TeV

…is shown. All limits quoted are observed minus 1σ theoretical signal cross section uncertainty.

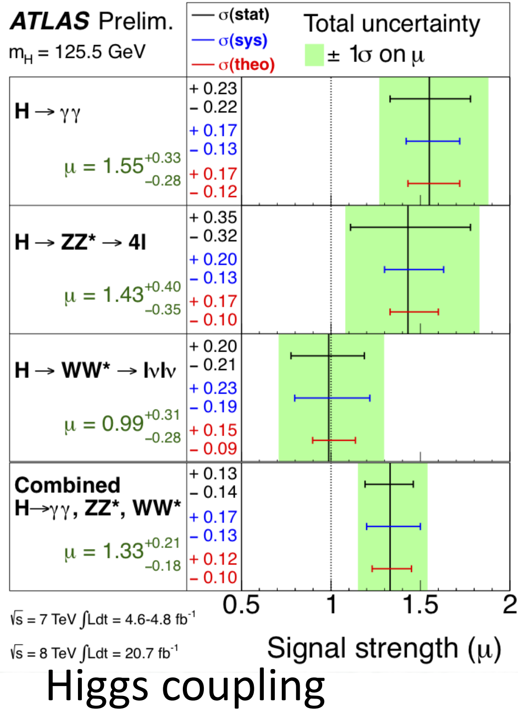

Higgs coupling

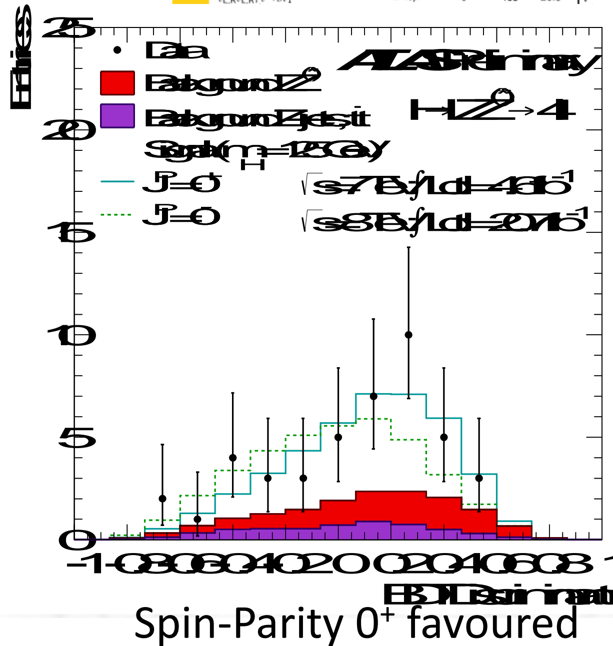

Spin-Parity 0^+ favoured

- Higgs – Great discovery of the century
- Need high statistics
  - Study of properties
  - Search for “something” in TeV mass region

Schedule for HL-LHC

2009

Start of LHC

Run 1: 7 and 8 TeV centre of mass energy, luminosity ramping up to few 10^{33} cm^{-2} s^{-1}, few fb^{-1} delivered

2013/14

LHC shut-down to prepare machine for design energy and nominal luminosity

IBL installation

Run 2: Ramp up luminosity to nominal (10^{34} cm^{-2} s^{-1}), ~50 to 100 fb^{-1}

2018

Injector and LHC Phase-I upgrades to go to ultimate luminosity

LHC

Run 3: Ramp up luminosity to 2.2 x nominal, reaching ~100 fb^{-1} / year accumulate ***few hundred*** fb^{-1}

~2022

Phase-II: High-luminosity LHC. New focussing magnets for very high luminosity with levelling

HL-LHC

Run 4: Collect data until > ***3000*** fb^{-1}

2030

Inner Detector Upgrade (HL-LHC)

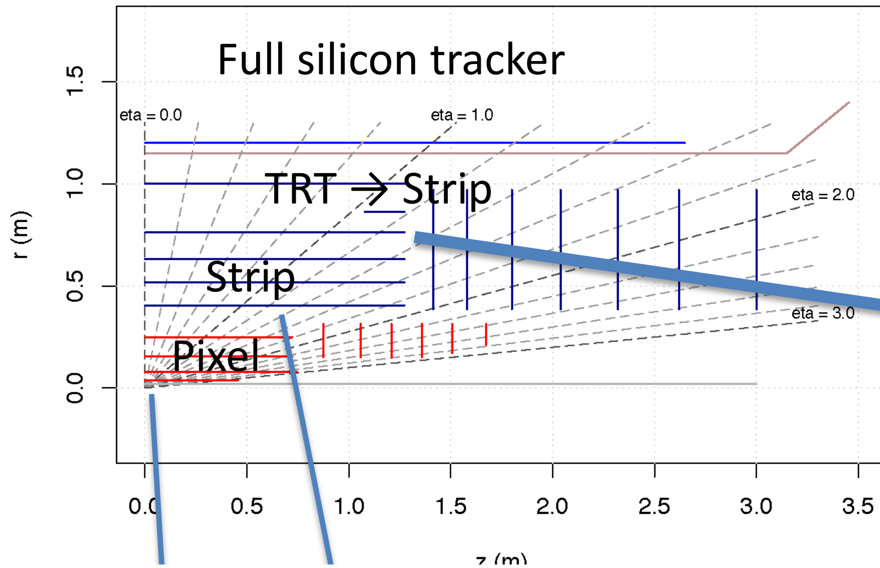

Strip sensor module, example

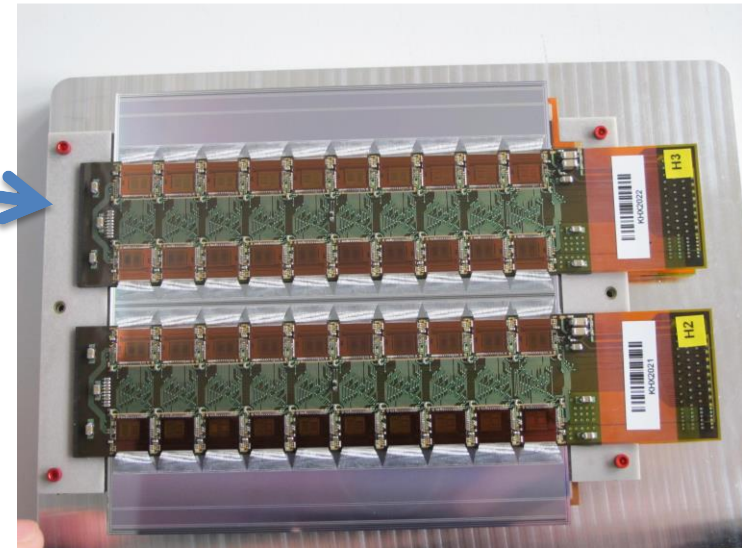

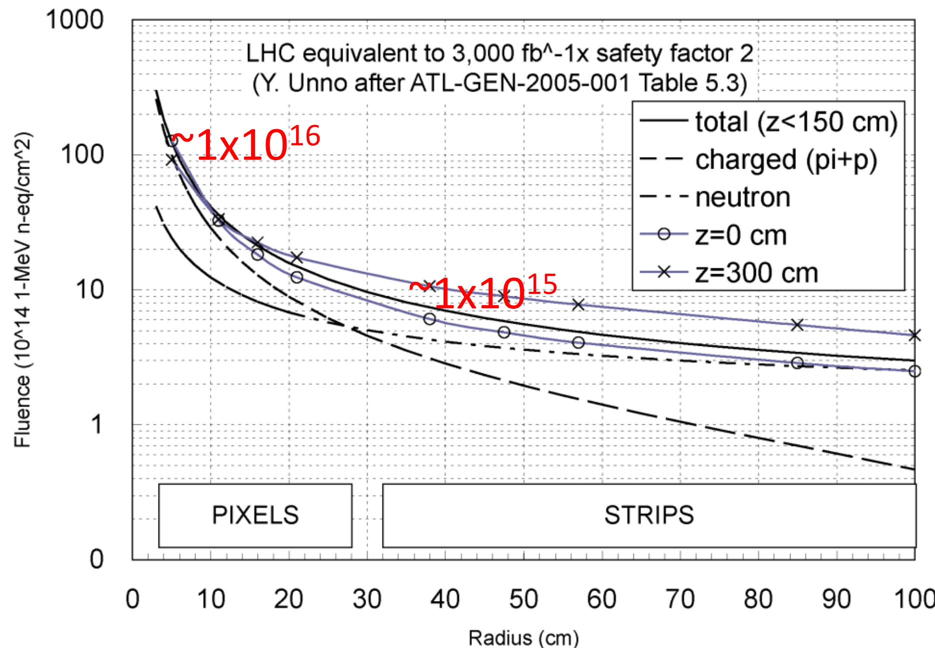

- 2022 – Full tracker replacement
  - Area: ~200 m^2
  - Silicon strips: ~1×10^{15} neq/cm^2
- Silicon sensors
  - Max. 1000 V operation
  - Full depletion might not be possible…

Cost-effective n-in-p planar sensor

n-in-n

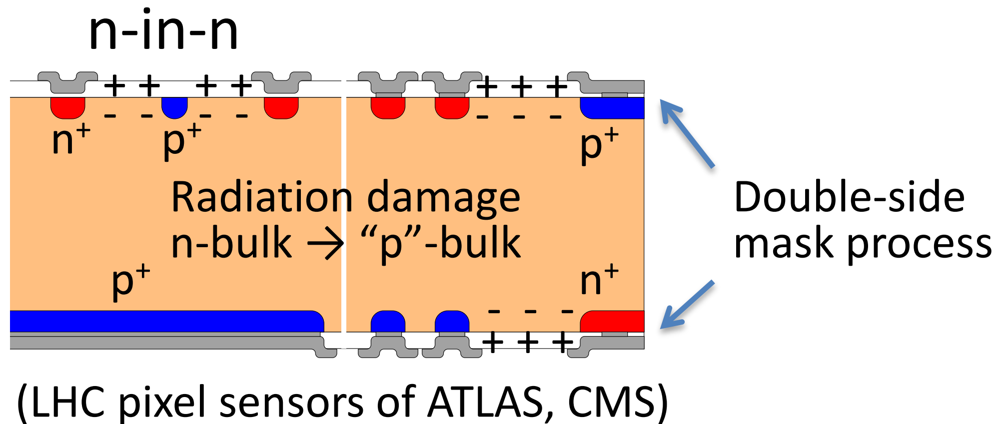

(LHC pixel sensors of ATLAS, CMS)

n-in-p

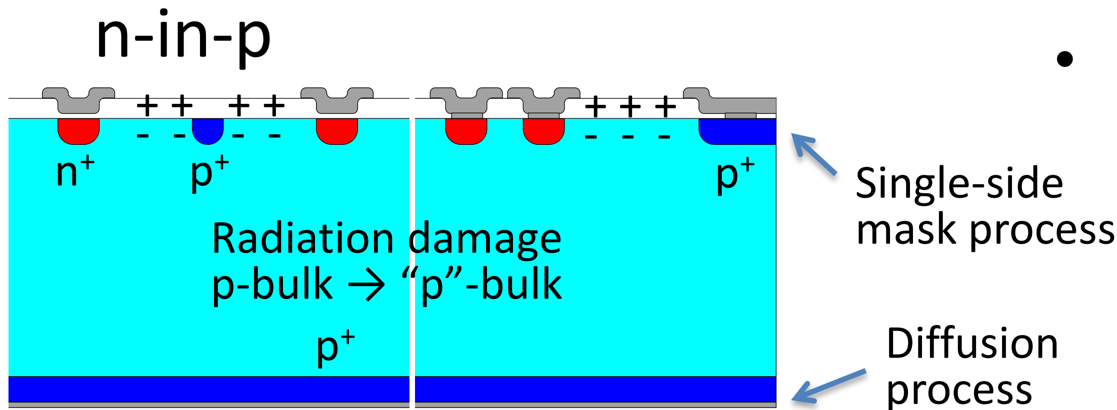

ATLAS choice for strip sensors for HL-LHC

- for heavy radiation environments
- Bulk radiation damage
  - one way to be "p" type
- n^+ readout
  - p-n junction to allow getting signals from "partially" depleted sensor
- Special in n+ readout
  - conductive layer in the surface
    - ~MΩ/square
    - due to the electrons attracted to the oxide trap/fixed charges
    - no junction effect at the n^+ implant
  - the electron layer must be
    - interrupted (p-stop), or
    - cancelled (p-spray)

n-in-p sensors for HL-LHC

- Sensors with the p-stop isolation
- Operable to 1000 V bias voltage.
  – Equivalently, suppressing "microdischarge" breakdown up to ~1000 V
- How?
  – Those 0, 1, 2, backed by 3
  – In addition, protection against beam splash: punch-through-protection (PTP) structure

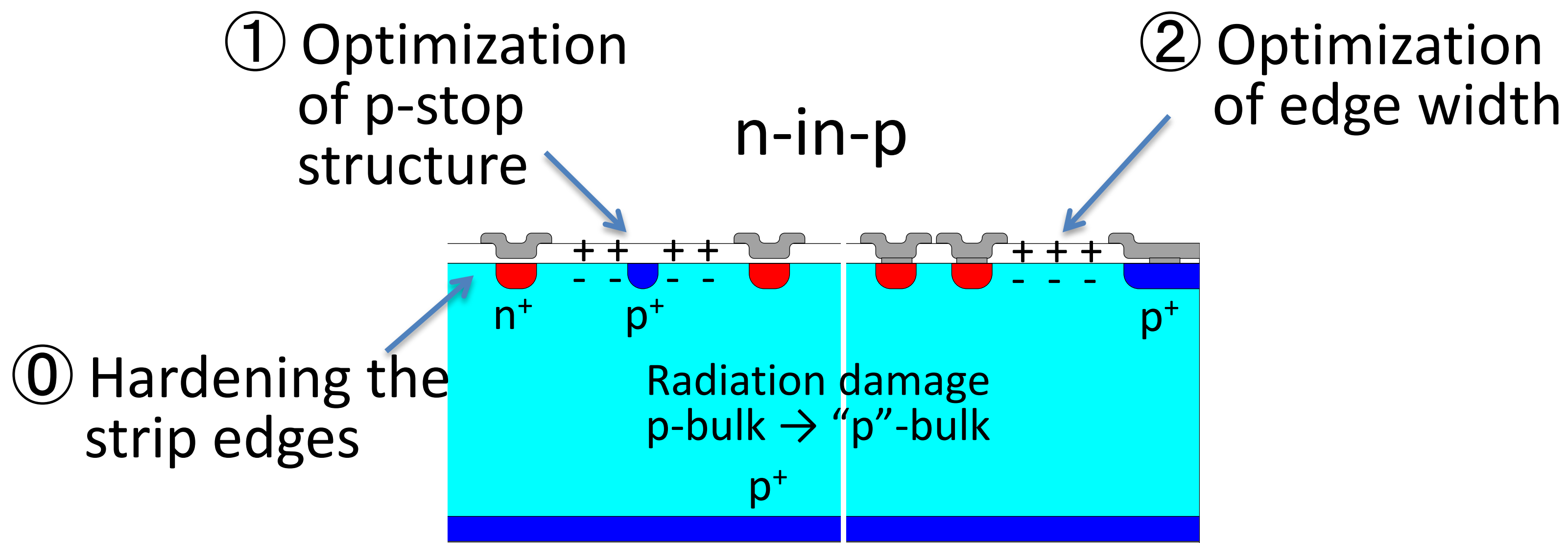

Study of required edge width

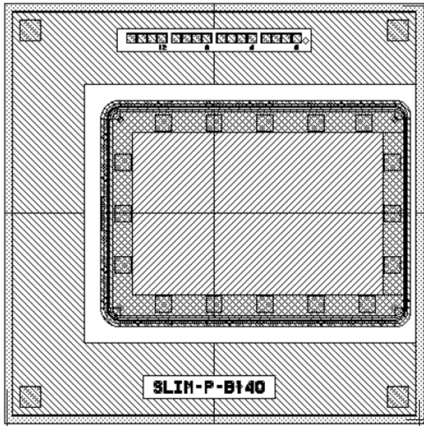

Width varied at one edge

- Results are from N-type wafer
- Thickness (as is, thinned)
  - 320 (W5), 200 (W7,13) µm
- Edge implantation
  - N+ or P+

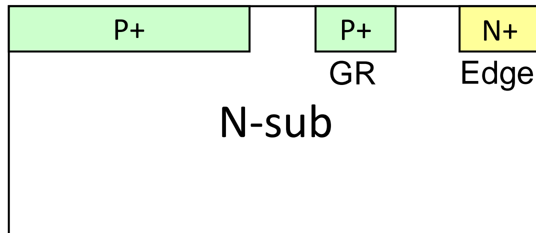

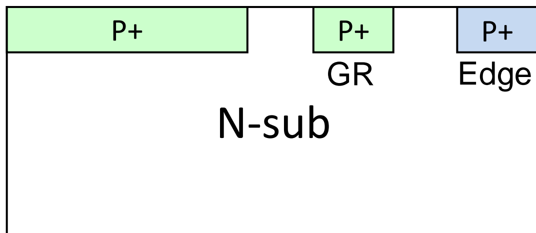

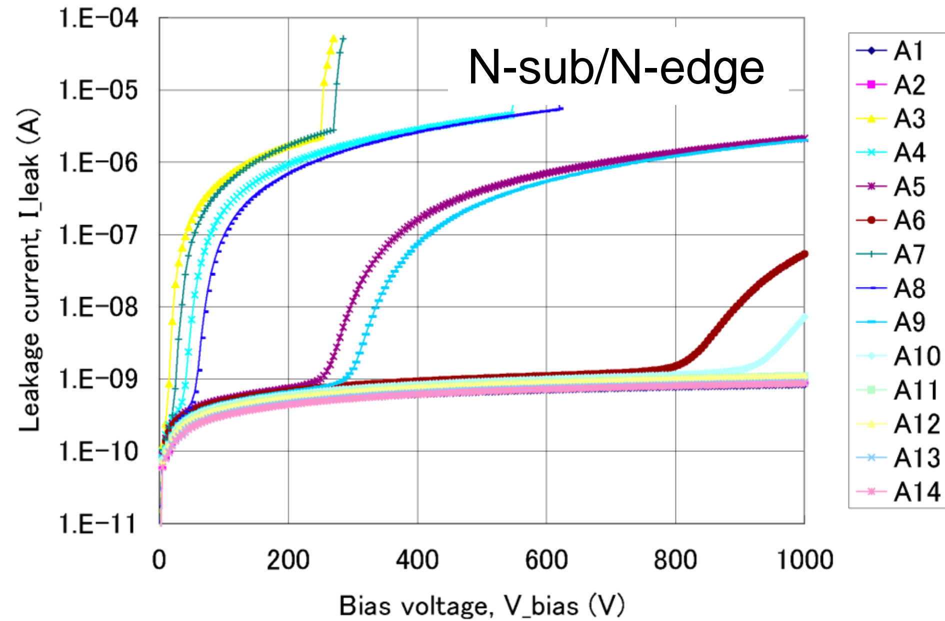

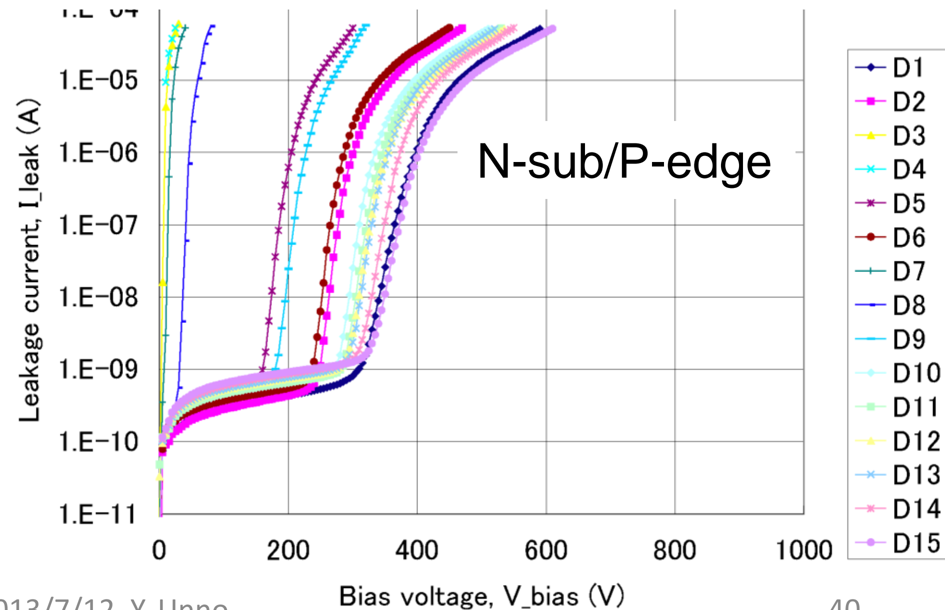

Underlying physics of the edge width

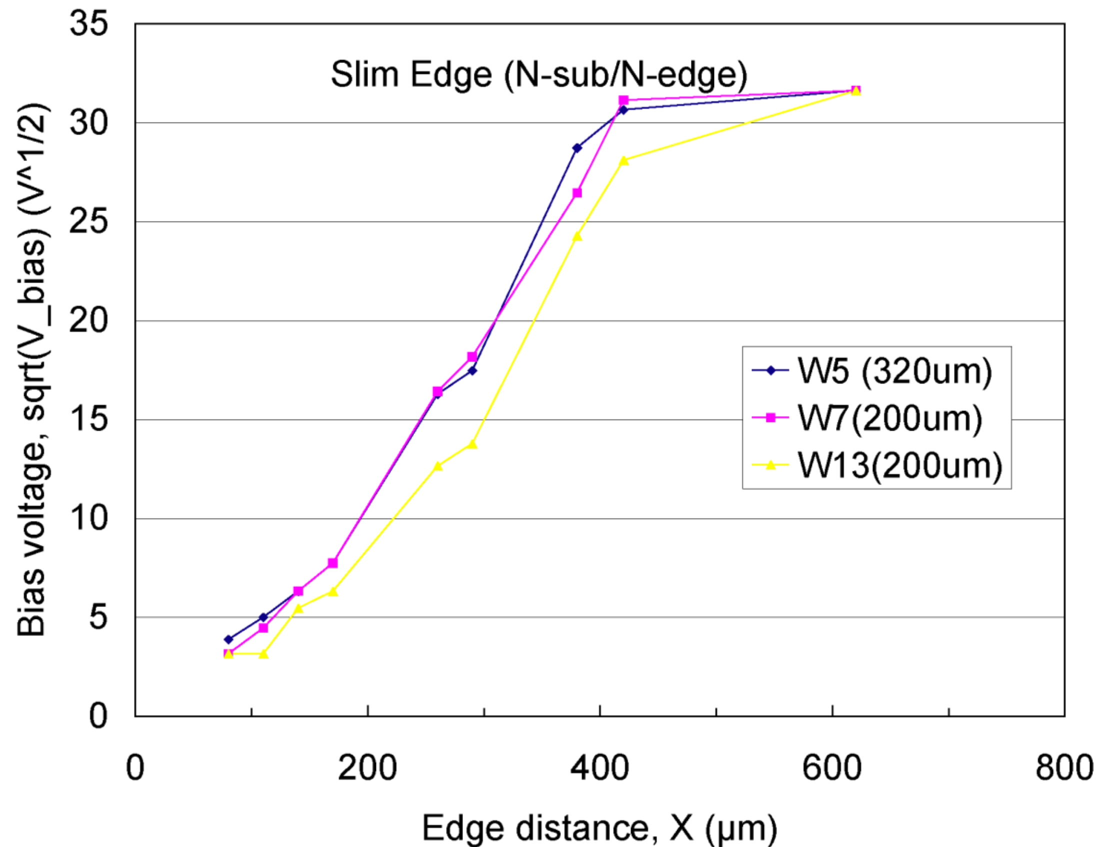

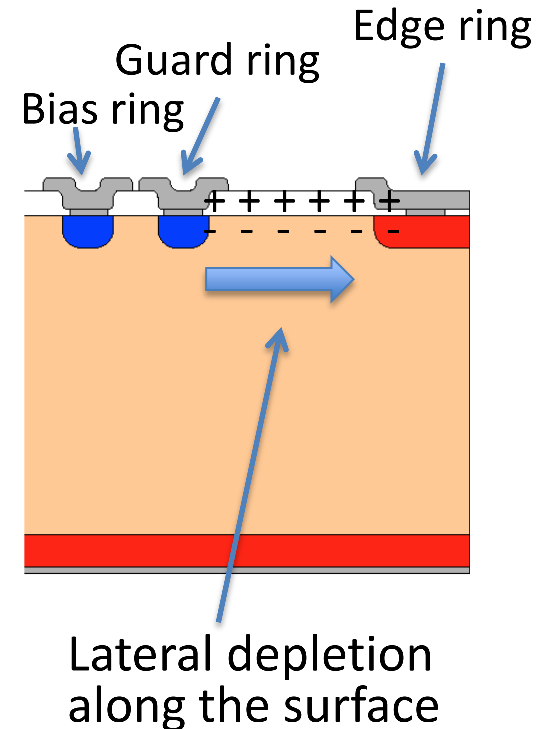

- Square root of V_bias is linearly dependent on the edge distance
  - Reflecting the depletion along the surface
- Distance can be ≤500 μm for the bias voltage up to 1 kV
- … Different story if the side wall is implanted e.g., - active edge

Required width after Irradiation

S. Mitsui et al, NIMA 699 (2013) 36-40

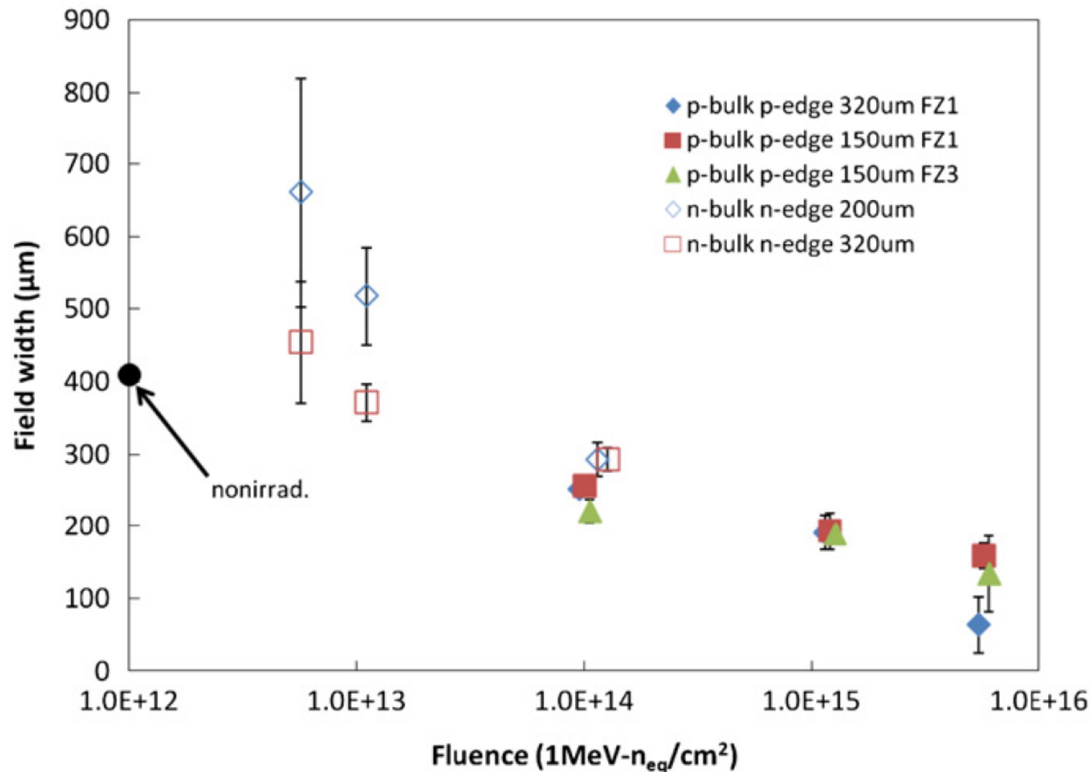

Fig. 5. Fluence dependence of field width hold up to 1000 V.

- Required width is ~450 µm to hold 1000 V.
  - At around 1x10^{13}, the required edge space is more than 450 µm, but also the depletion voltage is decreased less than that of non-irrad. and anyway it is much less than 1000 V.
  - At higher fluences, the required width is less than that of the non-irrad.

P-stops between N-implants

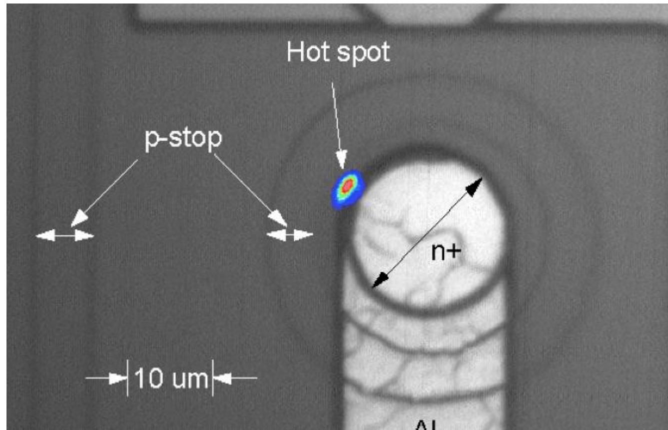

- Problems - Hot spots
  - IR image overlaid on visual image
  - Microdischarge = Onset of leakage current
- How to optimize the structures to reduce the electric fields?

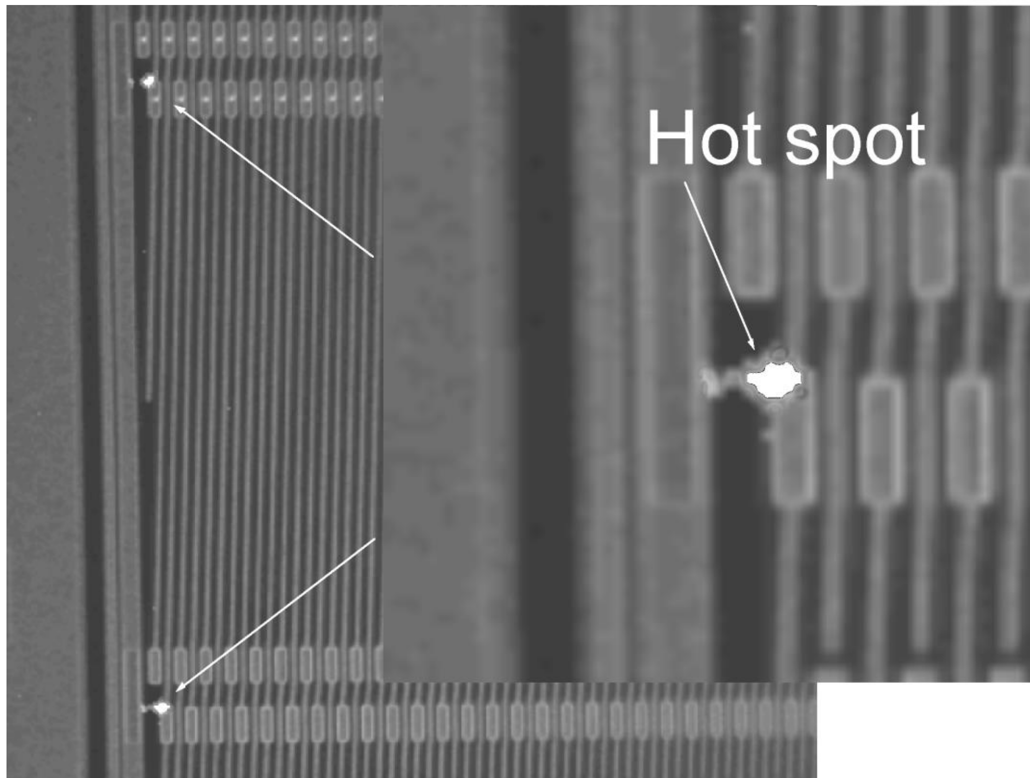

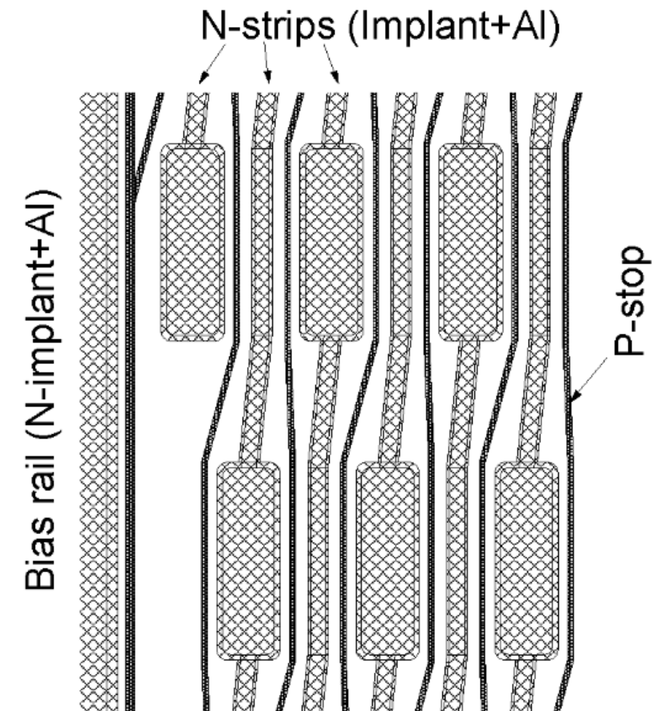

P-stop Structures Optimization

- TCAD simulations

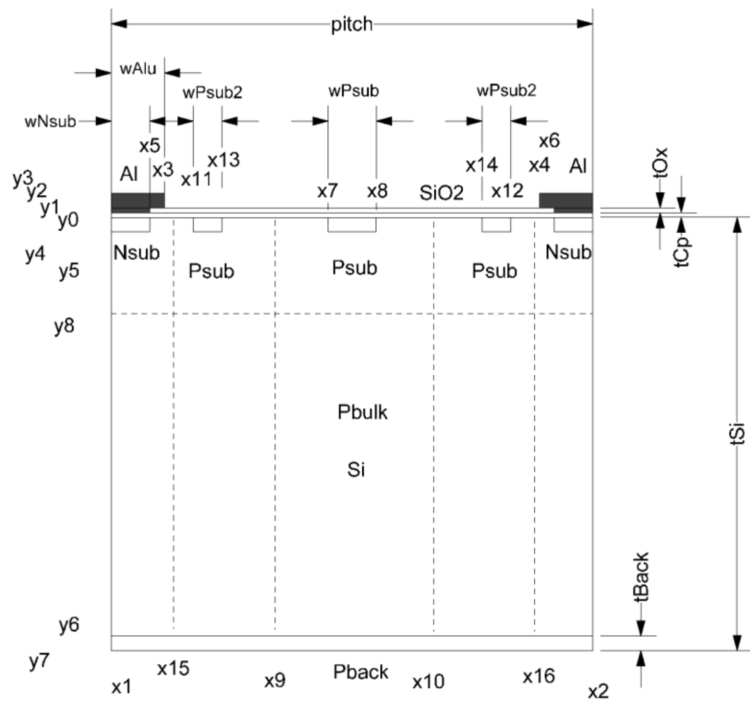

Y. Unno et al., Nucl. Instr. Meth. A636 (2011) S118–S124

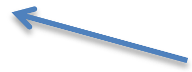

… and comparison with test structures

Optimization of the p-stops

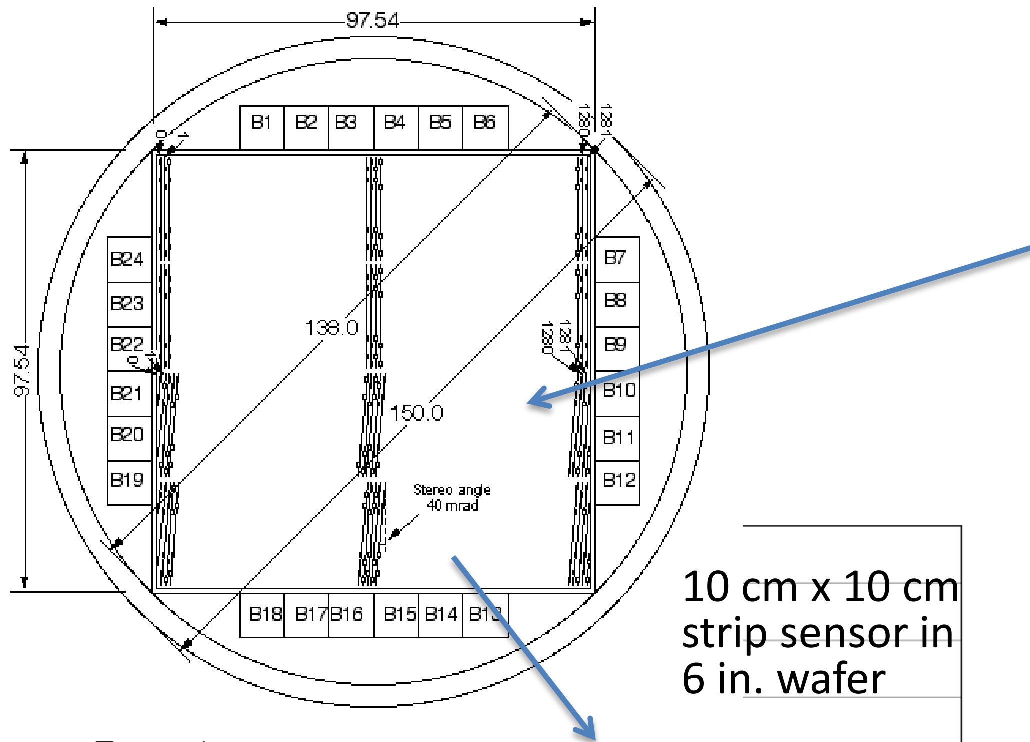

10 cm x 10 cm strip sensor in 6 in. wafer

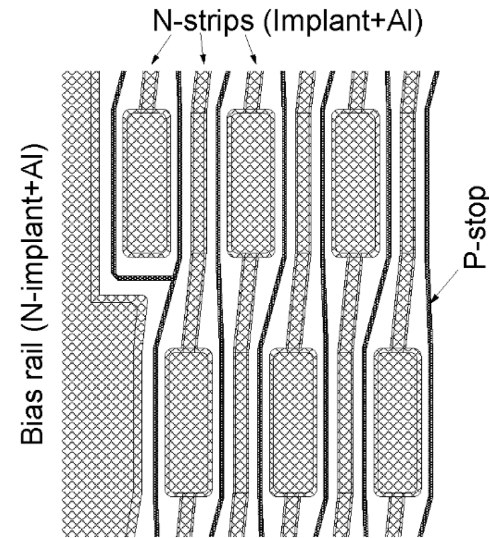

Stereo strip section

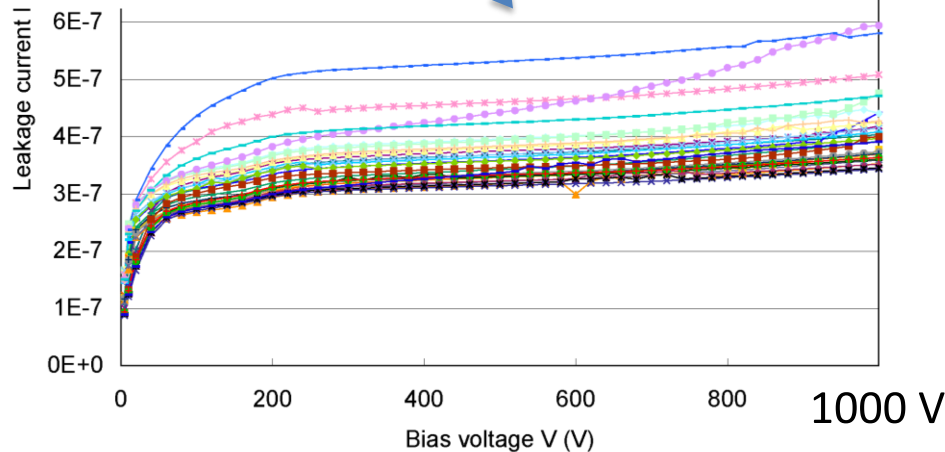

- P-stop
  - away from the n-implant
  - symmetric location
- N-implant
  - pitch not too narrow nor not too wide
- Once known, simple.

Technology CAD (TCAD)

- TCAD started to build the links between the
  - semiconductor physics and electrical behavior
  - to support circuit design
- Modern TCAD consists of
  - Process simulation, and
  - Device simulation
- Originated from the work of
  - Prof. Robert W. Dutton and his group at Stanford Univ.
- Widely used in semiconductor industry
  - to reduce the development cost and time
  - to understand the physics behind
    - that is even impossible to measure
- TCAD: Computer Aided Design for Semiconductor Technology

- The core is the “Finite Element Analysis”.
  - The numerical analysis method with modern computer.

MOS transistor

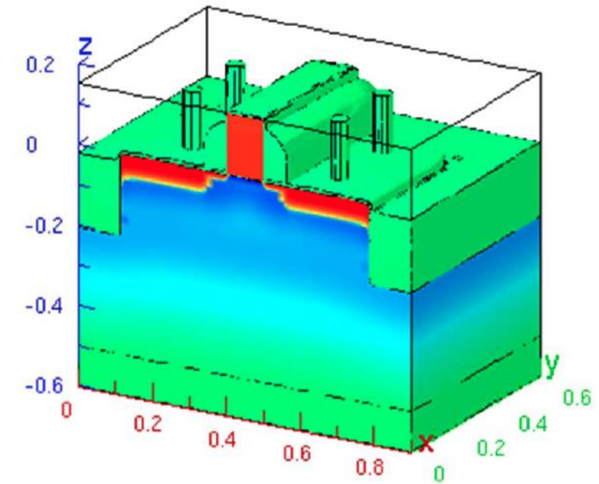

Process simulation

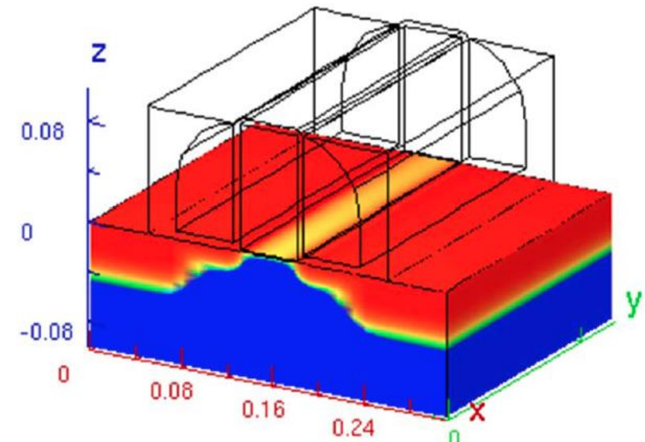

Device simulation

Brief History

Prof. Robert W. Dutton
(from Stanford TCAD Home page)

1977: Prof. Dutton, Stanford
Process/Device simulator
SUPREM-I (1D)/PISCES
1979: Technology Modeling Associates (TMA/Synopsys)
TSUPREM4 (2D)/MEDICI
1989: Silvaco International
ATHENA (2D)/ATLAS
1989: Integrated Systems Engineering AG (ISE)/Synopsys)
DIOS (2D)/DESSIS
1992: TMA
TAURUS (3D TSUPREM4/DEDICI)
1993: Prof. Law, Florida
Process sim: FLOOPS (3D)
2002: ISE
FLOOPS (3D)
2005: Synopsys
Sentaurus (3D TAURUS)

TMA⇒AVANT!/1998⇒Synopsys/2001
ISE⇒Synopsys/2004

In Japan,
1996: 3D HyENEXSS (Selete/TCAD Int.)
Selete: Consortium of 10 semiconductor co.
2011: 3D HyENEXSS (Selete)
Project ends

Process Simulator | Device Simulator

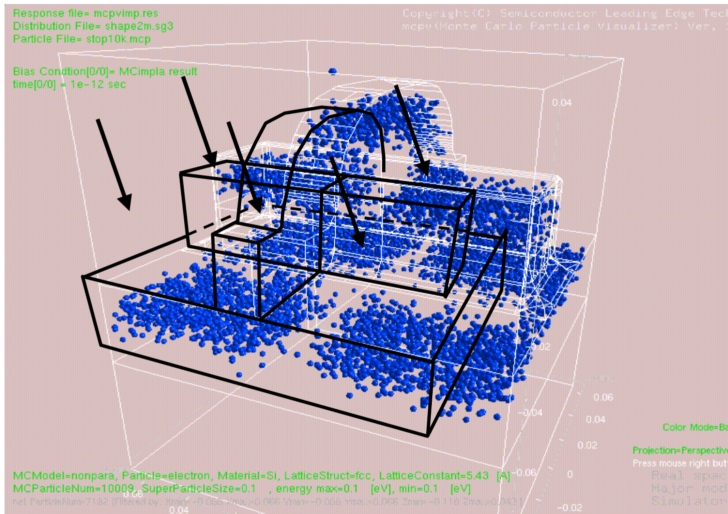

ion-implantation process (M.C.-model)

- Process steps
  - Oxidation
  - Deposition
  - Etching
  - Ion implantation
  - Annealing
- Mostly for process experts
  - Unless you know the process parameters, you have no way to simulate.

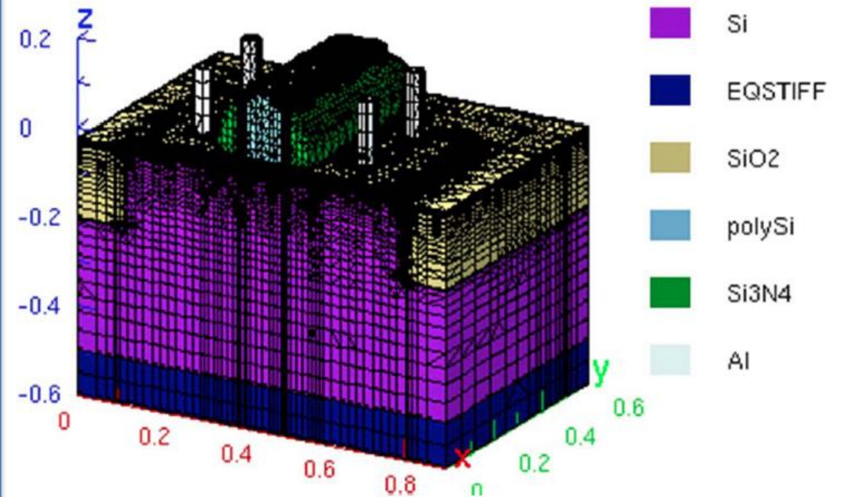

- Solving equations
  - Poisson eq. (ψ, n, p)
  - Current continuity eq. *Jn*, *Jp* (ψ, n, p)
  - Heat conduction eq. ("Drift Diffusion model) (TL)
  - …
- Four equations and four variables
  - potential ψ, electron-density n, hole-density p, and lattice-temperature TL

Caveat

- Jungle of semiconductor physics models and parameters
  - Device simulator e.g.,
  - Transport models
  - Mobility models
  - Generation-recombination models (SRH, Auger, II, trap, surface…)
    - SRH: Shockley-Read-Hall model
    - II: Impact Ionization model
- Finite Element method
  - 3D vs. 2D
    - 3D: Usually "very" time consuming
    - 2D: Most of the cases, good enough
  - Meshing: resolution vs. time
  - Convergence of calculations
    - Try and error for finding best procedures (method, physics model)
- The real caveat is
  - "What you get is what you put."
  - Although semiconductor industry is trying to simulate perfectly, we may still miss models, e.g., radiation damages

TCAD Simulations

- Semiconductor Technology Computer-Aided Design (TCAD) tool
  - ENEXSS 5.5, developed by SELETE in Japan
  - Device simulation part: HyDeLEOS
- N-in-p strip sensor
  - 75 µm pitch, p-stop $4x10^{12}$ cm^{-2}
  - 150 µm thickness
  - p-type bulk, $N_{eff}=4.7 \times 10^{12}$ cm^{-3}, $V_{FDV}=80$ V at 150 µm
- Radiation damage approximation:
  - Increase of acceptor-like state → Effective doping concentration
  - Increase of leakage current → SRH model
  - Increase of interface charge → Fixed oxide charge

Bulk leakage current

After irradiation, the current increases as a function of fluence
$\Delta I/V \sim \alpha \times \phi (n_{eq}/cm^2)$
$\alpha \sim 4 \times 10^{-17}$ (A/cm) : damage constant
E.g.,
Volume = 75 μm x 1 μm x 150 μm = 1.13 x 10^{-8} cm^3
ϕ=$1x10^{15}$ n_{eq}/cm^2
ΔI ~45 nA

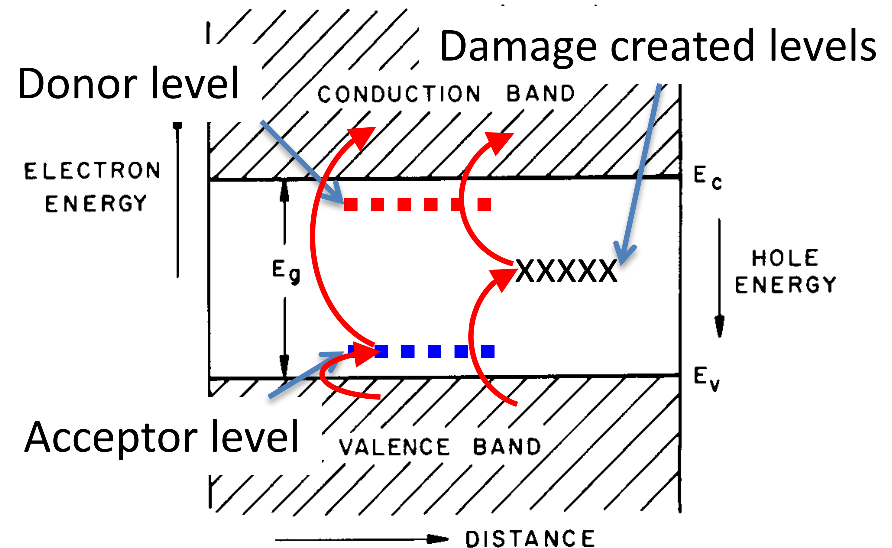

Fig. 6 Simplified band diagram of a semiconductor.

- Community has a view that
  - the leakage current increases with an introduction of levels near the middle of the forbidden band,
  - with the energy of band gap being half (of the full gap), the leakage current flows order of magnitude larger…
- Unfortunately, we have no freedom to change/add a program to the ENEXSS, but
  - we can simulate the leakage current by modifying the model parameters to an unrealistic world…

Shockley-Reed-Hall (SRH) Model

- Leakage current: SRH model
  - Generation-recombination of carriers (electrons and holes) by thermal effect
  - A_n, A_p : model parameters
    - Decrease them as though increasing temperature

$$U_{SRH} = \frac{n_i^2 - pn}{\tau_p\left(n+n_i\right)+\tau_n\left(p+n_i\right)}$$

$$\tau_{n,p} = A_{n,p}\left(\tau_{\min}^{n,p} + \frac{\tau_{\max}^{n,p} - \tau_{\min}^{n,p}}{1+\left(N / N_t^{n,p}\right)^{B_{n,p}}}\right)$$

n_i: intrinsic carrier density,

n, p: electron, hole carrier density

Radiation Damage Approximation

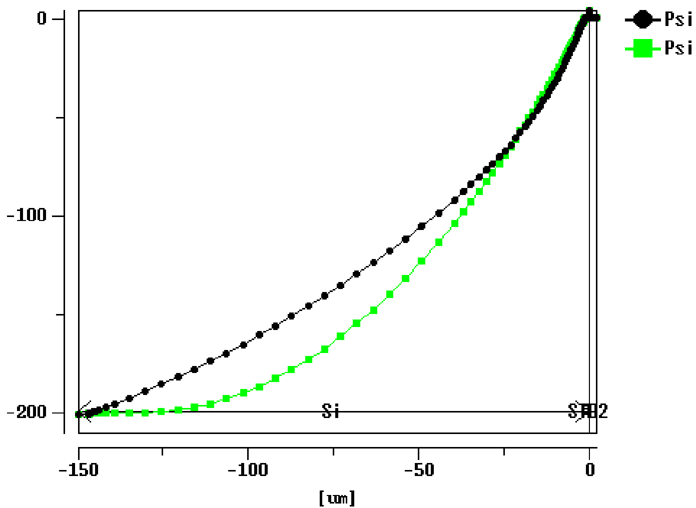

Backplane at 200 V

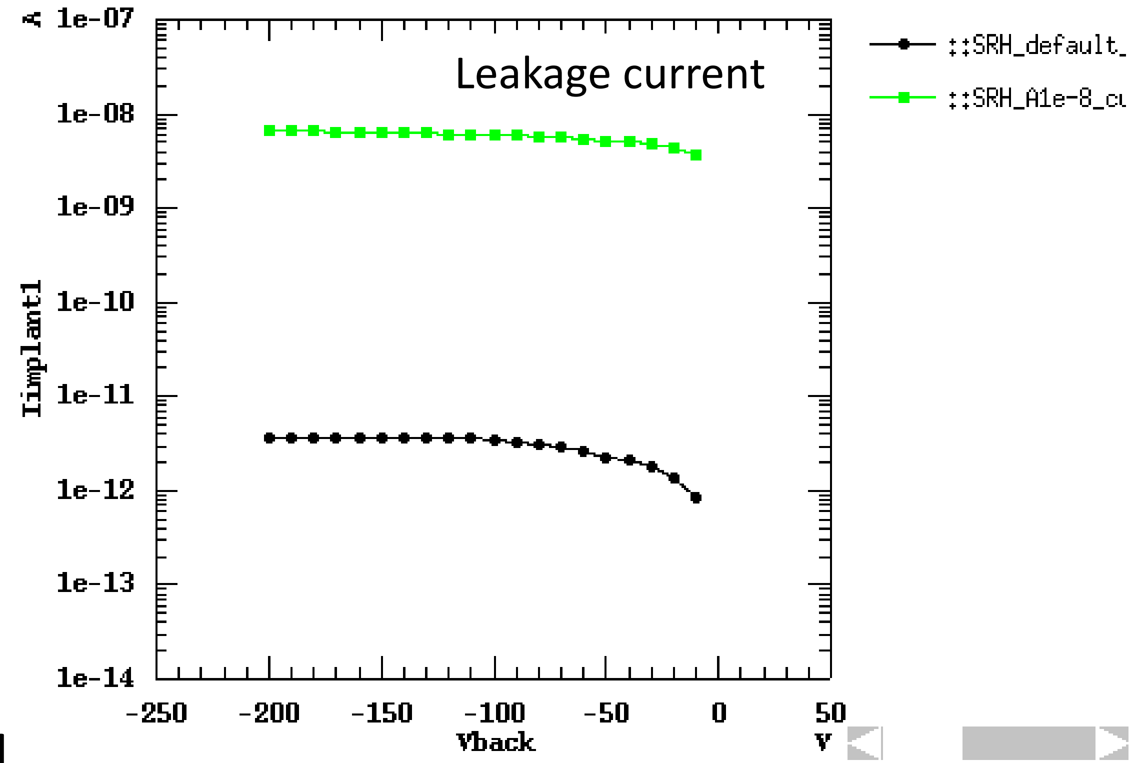

- Black: non-irrad.
  - $N_{eff}=4.7\times10^{12}$ cm^{-3}, A_n, A_p = 1.0
- Green: Irrad.
  - Increase of full depletion voltage, $N_{eff}=1.5\times10^{13}$ cm^{-3}
  - Increase of leakage current, A_n, $A_p = 1\times10^{-8}$

Interstrip Resistance, R_{int}

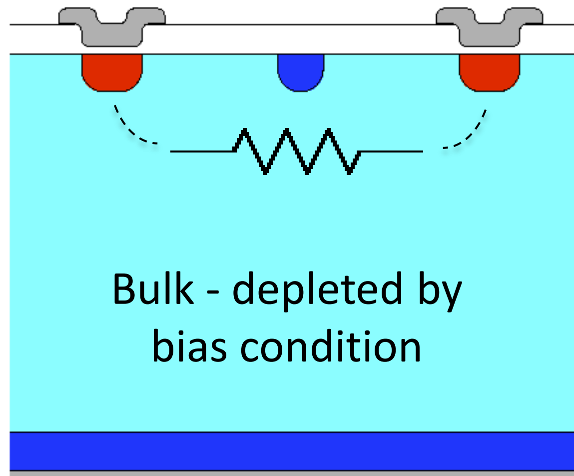

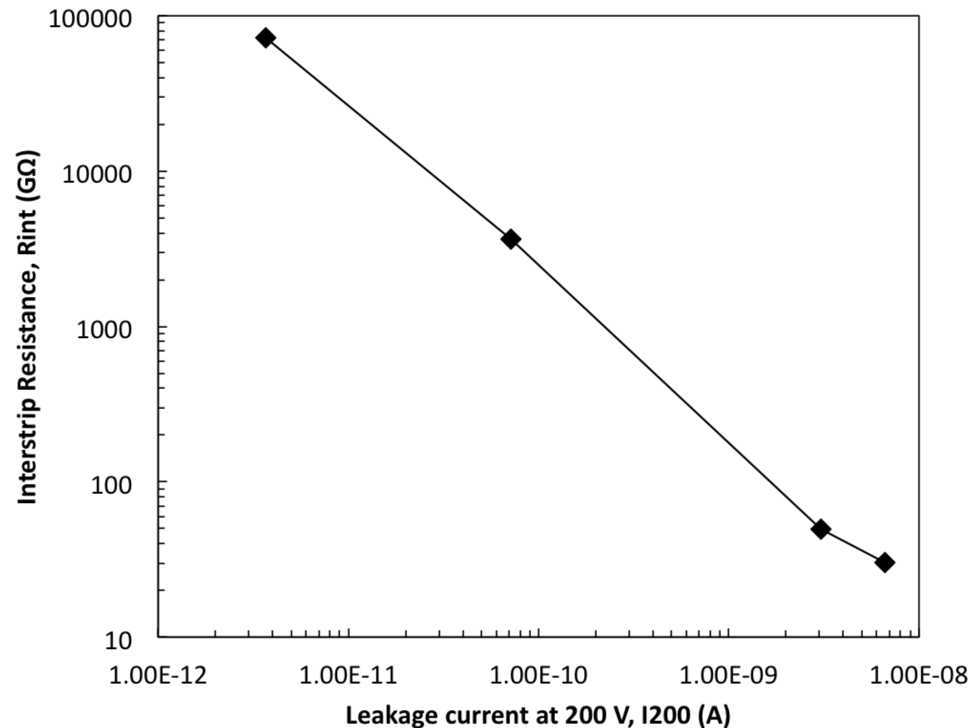

- Decrease of interstrip resistance after irradiation
  - is quantitatively explained by the increase of leakage current.
  - Other factors, the effective doping concentration nor the oxide interface charge, do not change the interstrip resistance.
  - In retrospect, it is natural that the current is the other manifestation of the resistance.

Electric potential of p-stop
- Introduction of Si-SiO_2 interface charge -

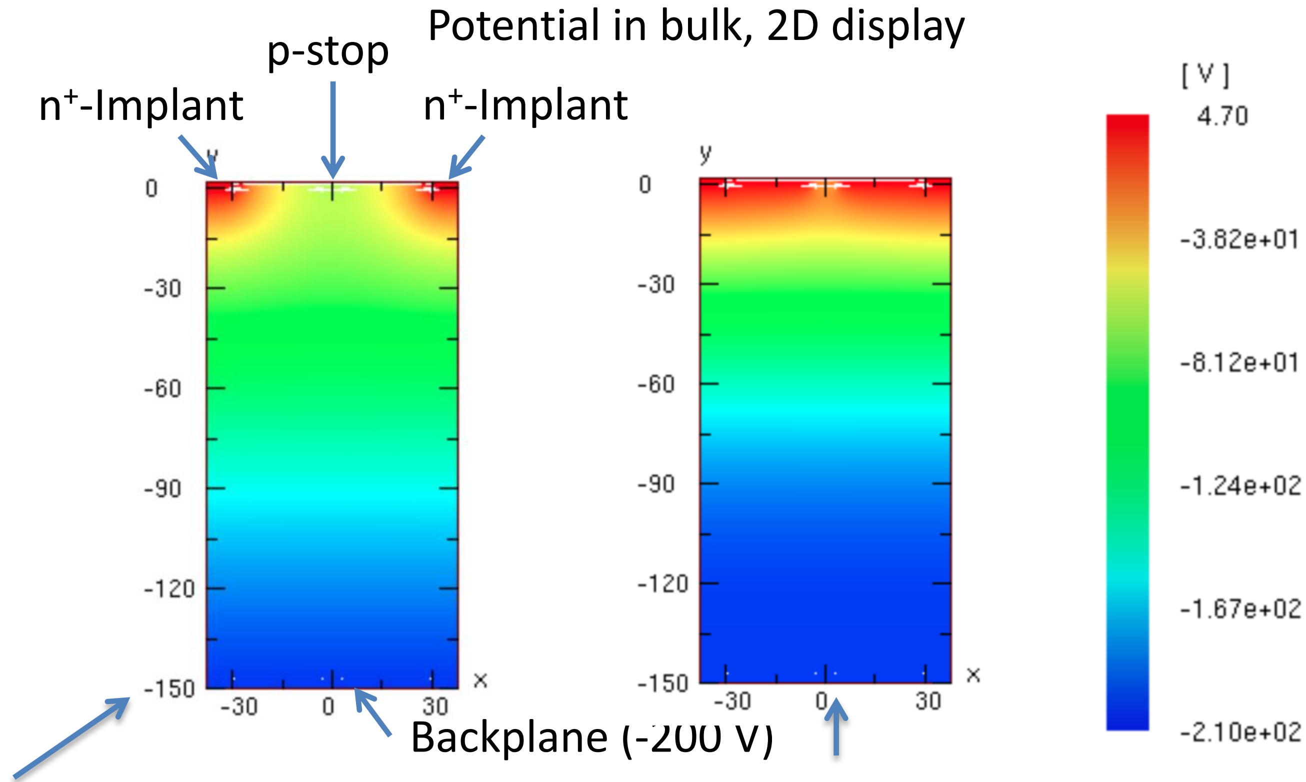

- Non-irrad:
  - N_{eff}=4.7×10^{12} cm^{-3},
  - SRH A_n, A_p=1.0,
  - Fixed Oxide Charge =1×10^{10} cm^{-2}
- Irrad:
  - N_{eff}=1.5×10^{13} cm^{-3},
  - SRH A_n, A_p=1×10^{-8} ,
  - Fixed Oxide Charge =1×10^{12} cm^{-2}

Electric Potential between Strips

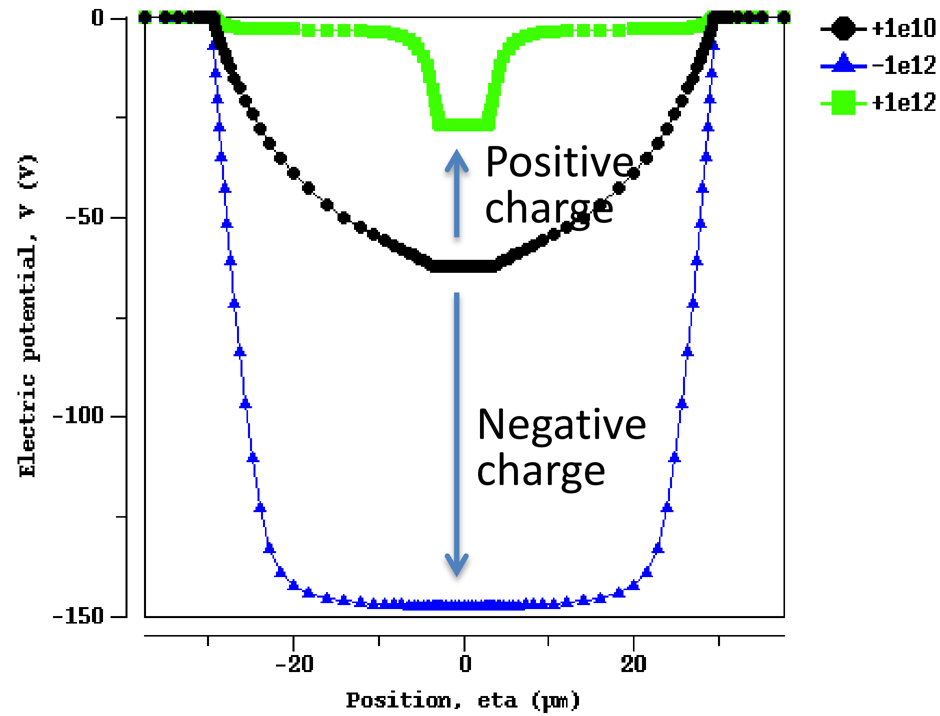

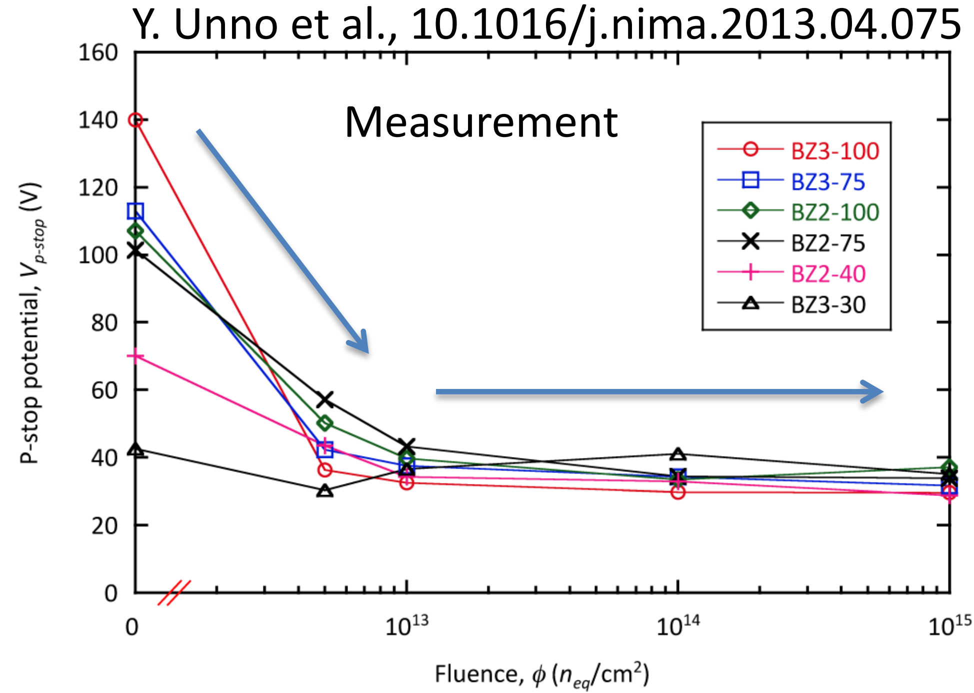

- Electric potential of p-stop
  - decreases as the interface charge increases positively,
  - increases as the interface charge increases negatively.
- Measurement confirms that the interface charge is positive.

Breakdown at High Voltages

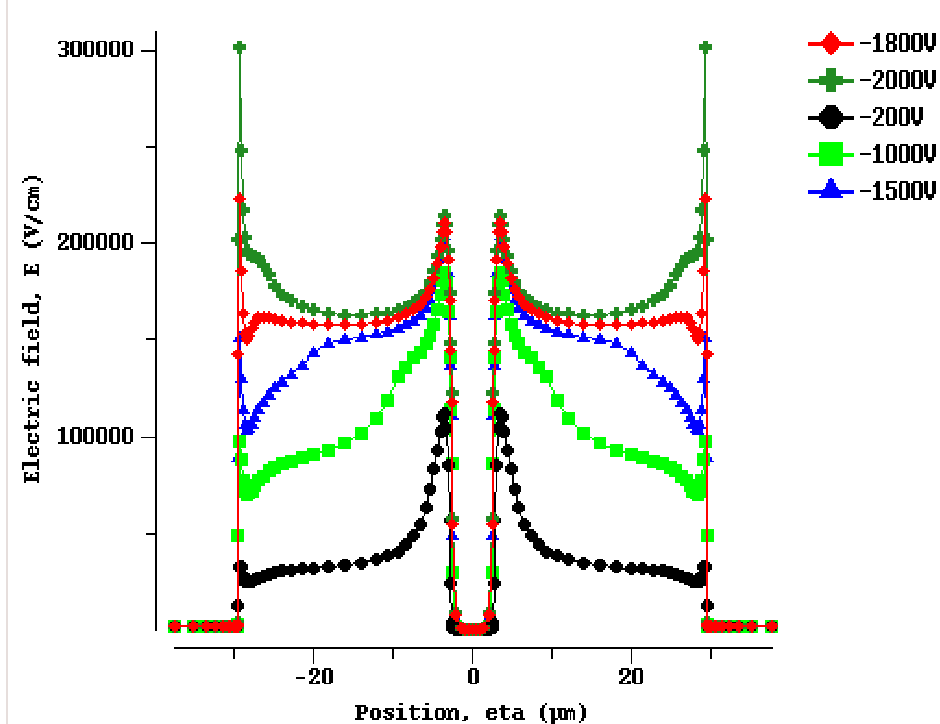

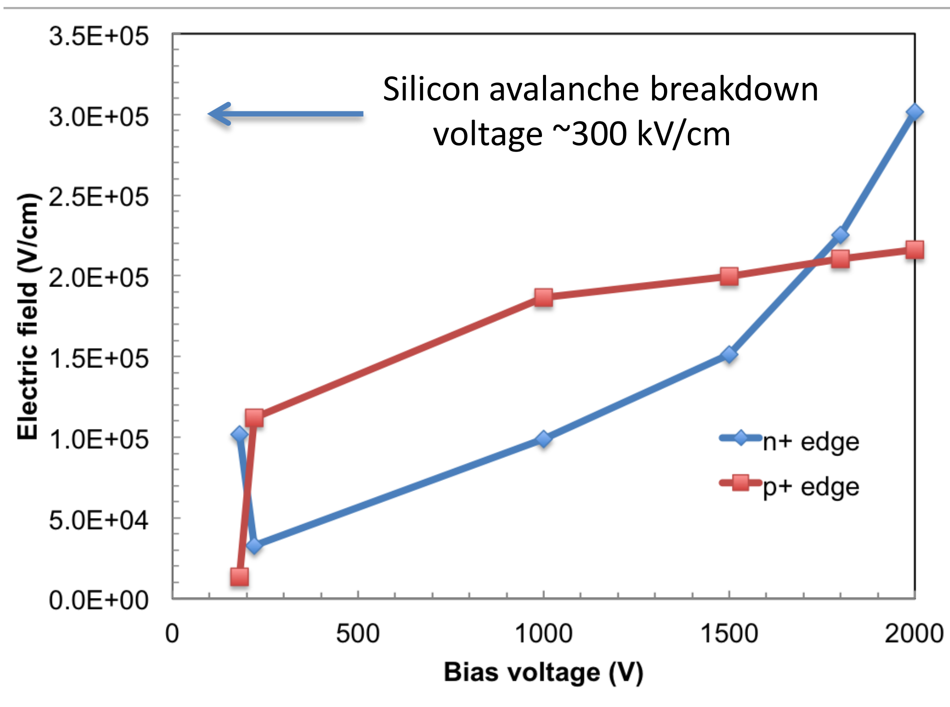

- Under the “Irradiated” condition
- Breakdown occurs at high voltage at the n^+ edge, although the p-stop edge was the higher electric field initially.
- The rate to increase of the electric field at the p-stop edge is saturating at higher voltage.
- The p-n junction eventually overtakes the highest electric field by the time of breakdown.
- Why?

Insight into the physics

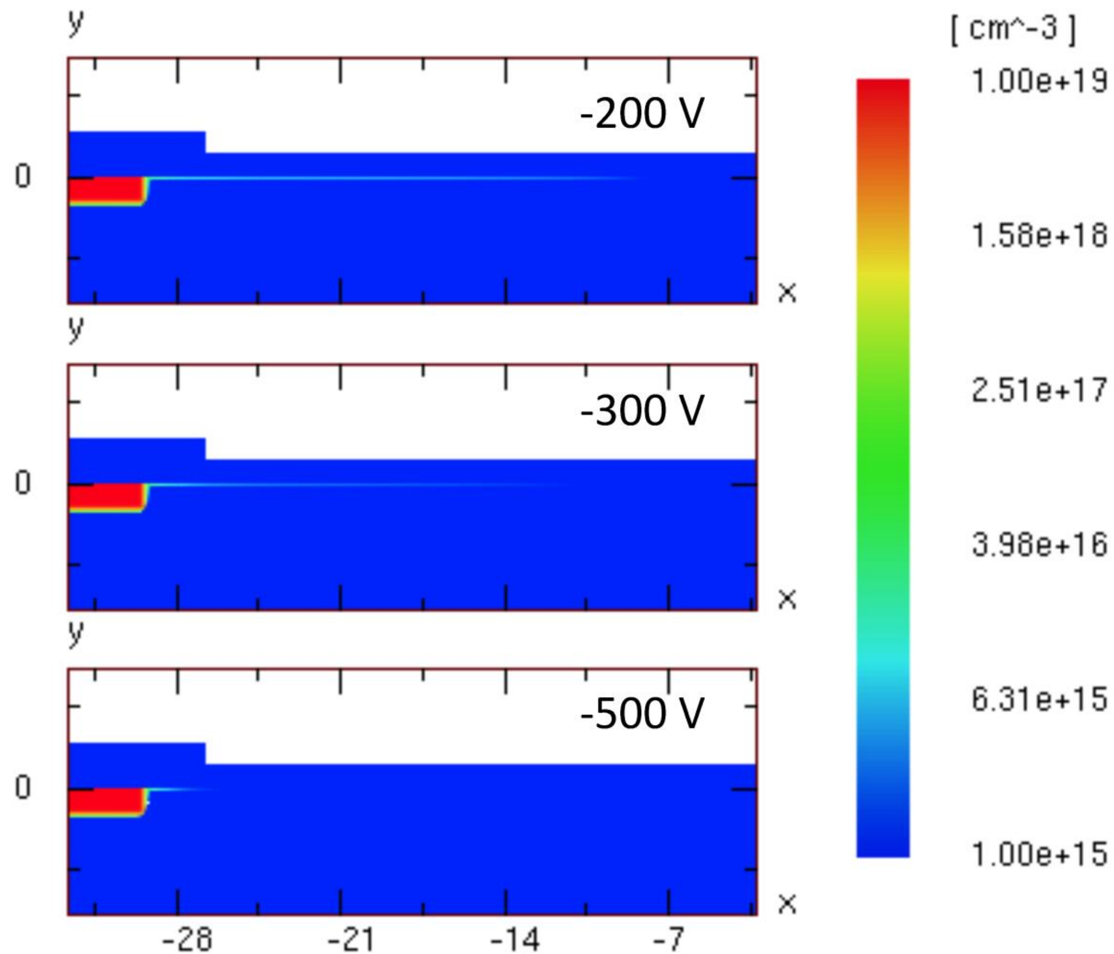

- Electron inversion layer is diminishing
  - as the bias voltage is being increased.
  - This also explains that in p-bulk the bias voltage helps to isolate the n^+ implants.
- Understanding the underlying physics is only possible with TCAD simulation, eventually …

Summary

- Brief overview of the current ATLAS silicon microstrip tracker (SCT)
  - ATLAS SCT strip detector is working well (so far).
- Issues and achievement of the LHC tracker
  - Radiation level, 2×10^{14} 1-MeV n_{eq}/cm^2
  - Radiation damage effects were identified
  - High voltage operation was designed up to 500 V
  - Strip edge hardening against high electric field was applied
- New technological achievement for the high-luminosity LHC tracker
  - Radiation level, $\sim 1 \times 10^{15}$ 1-MeV n_{eq}/cm^2
  - High voltage operation up to 1000 V
  - Minimum dead area in the edge is evaluated
- TCAD simulation
  - Simulating radiation damage effects with approximation
  - Very effective in understanding the underlying physics
- This is all about of the conventional planar silicon microstrip sensor...
  - You still have a lot of challenges ahead in different world/requirements.

Appendix

Signal from n^+ or p^+ strips

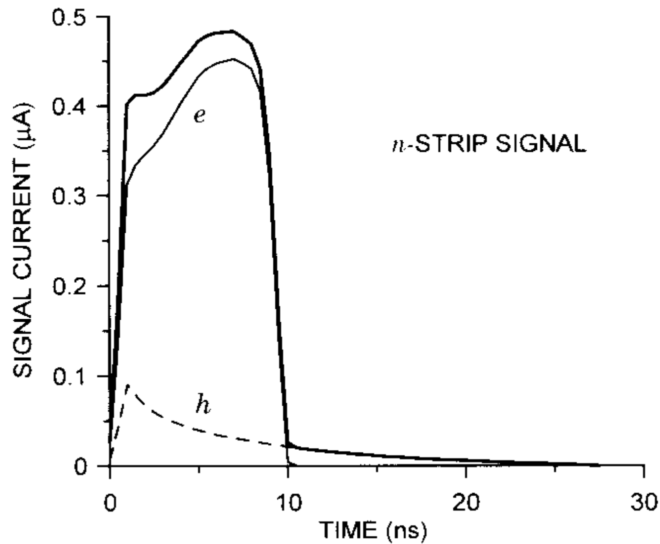

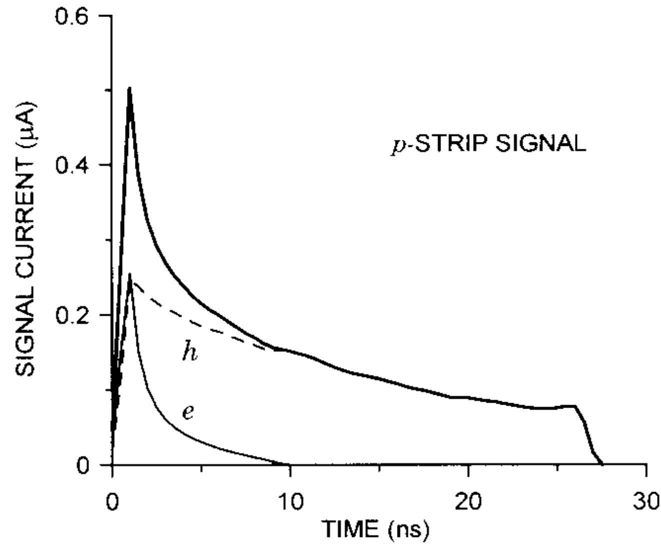

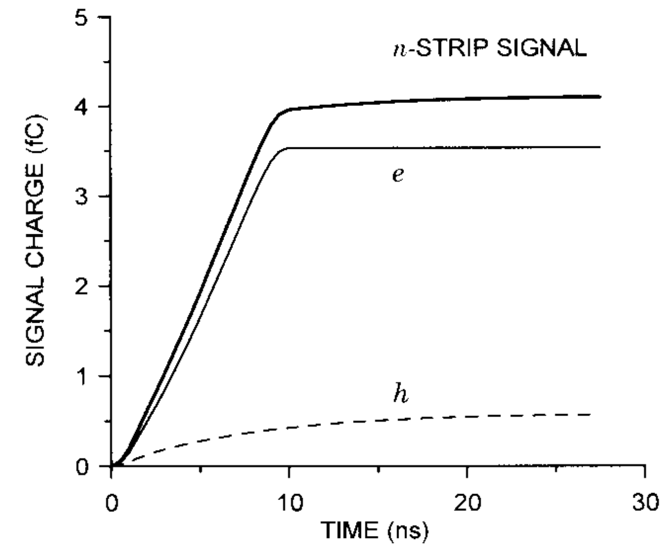

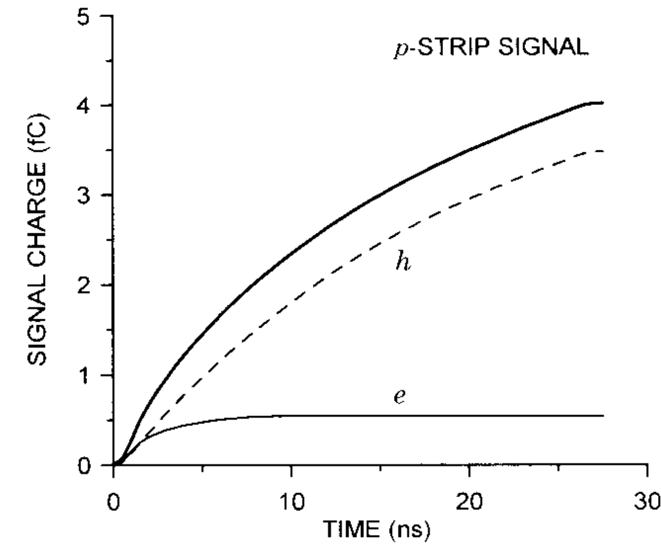

Signal ~ half of the carriers.

- High field around the strips
- Weighting field, mobility

n-bulk:

Low field toward n^+ strip

Punch-Through Protection (PTP) Structure

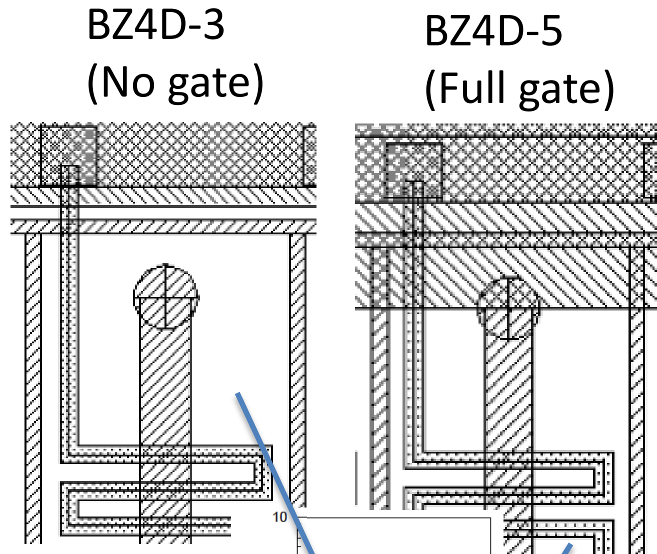

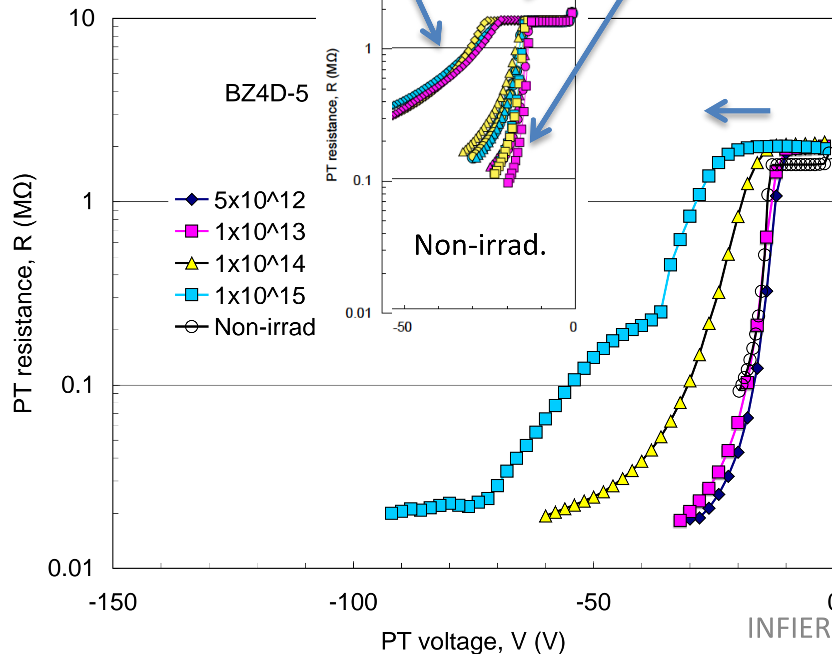

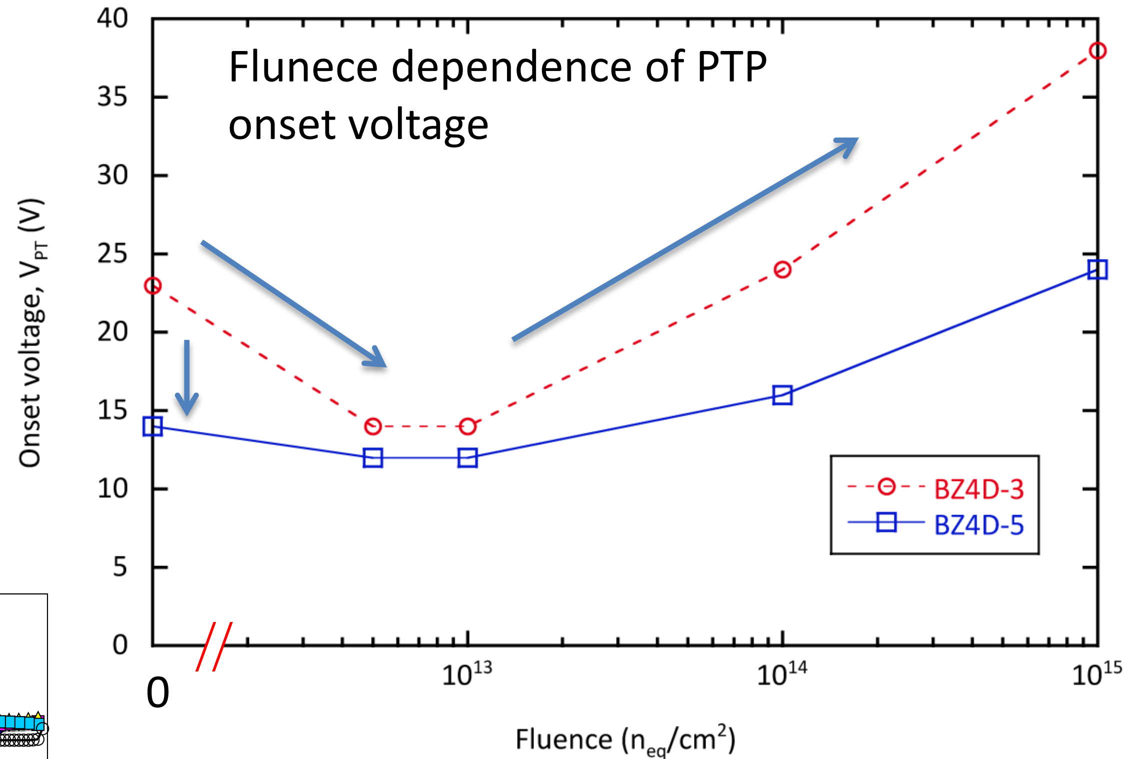

- "Full gate" induced PTP onset in lower voltages than "No gate".
- Onset voltage went down first and then started to increase.
  - What causes the transitions?

PTP Simulations

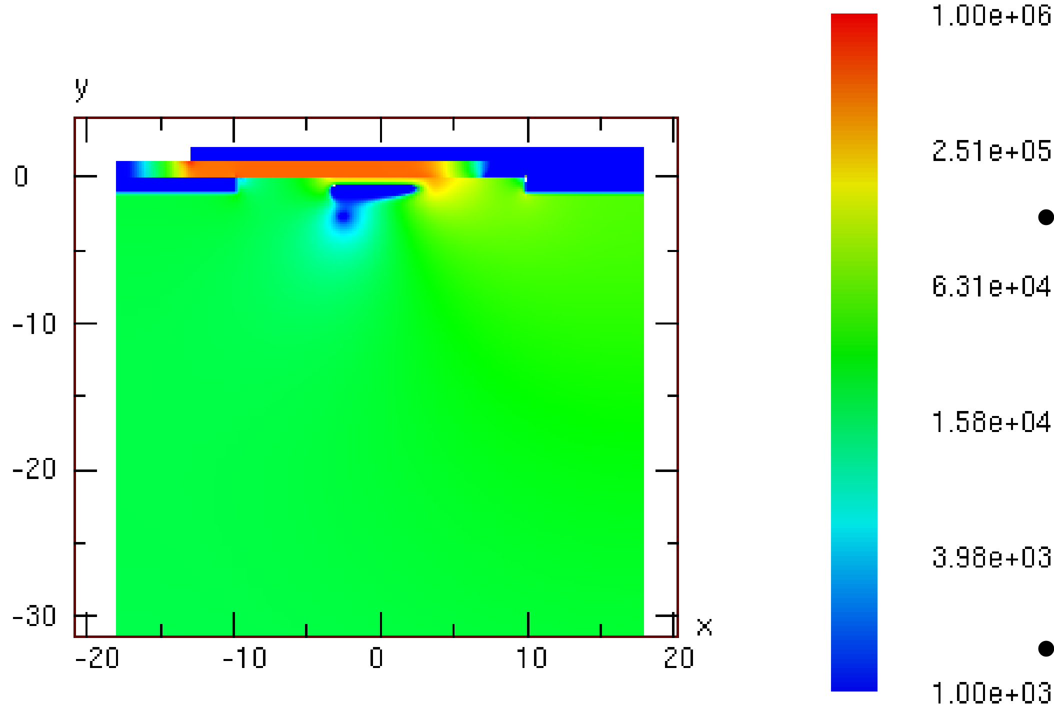

- TCAD
  - no bias resister in parallel
  - NPTP:"No gate"
  - Others: "Full gate"
- Parameters:
  - NB/DB: non/damaged bulk
  - LT/HT: lo/hi interface charge
  - LC/HC: lo/hi current
  - Non irrad: NB*LT*LC
  - Irrad: DB*HT*HC
- Irrad. simulation
  - Damaged bulk,
  - hi interface charge,
  - hi leakage current

TCAD simulation of
"Full gate" PTP, irradiated
Electric field at onset
when the backplane bias voltage at -200 V
V_{test} (left implant) at -50 V

PTP Simulations

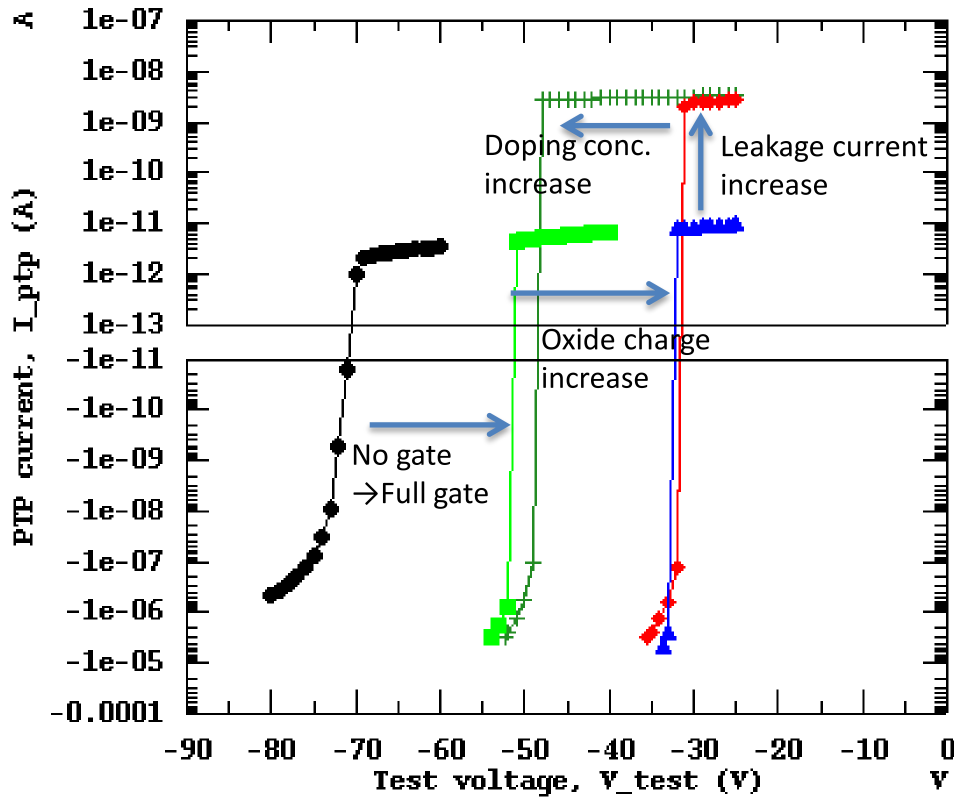

- The fluence dependence can be understood as the effect of
  - Build-up of the Interface charge and
  - Increase of acceptor-like levels.
- The systematic "offset"
  - difference between the 2D simulation and the 3D real.

- Onset voltage decreased as
  - No gate (black) → Full gate (colored)
  - Interface charge increased
- Increased as
  - accepter-like state increased